Supporting Information

The influence of hindered rotation on electron transfer and exchange interaction in triarylamine-triptycene-perylenediimide triads

Chantal Roger,[a] Alexander Schmiedel,[a] Marco Holzapfel,[a] Nikita N. Lukzen,[b] Ulrich E. Steiner,[c]* and Christoph Lambert[a,d]*

[a]*Institut für Organische Chemie, Universität Würzburg, Am Hubland, D-97074 Würzburg, Germany.*

[b]*International Tomography Center, Russia and Novosibirsk State Universit; Institutskaya 3a, Novosibirsk, Novosibirsk 630090, Russia*

[c]*Department of Chemistry, University of Konstanz, Universitätsstraße 10; 78464 Konstanz, Germany*

[d]*Center for Nanosystems Chemistry, Universität Würzburg, Theodor-Boveri-Weg, D-97074 Würzburg, Germany*

Contents

1. Synthesis

1.1. General

Commercially available compounds and standard solvents were purchased from either Acros, Chempur, Fluka, Honeywell, Merck or TCI and used without further purification. DCM, ethyl acetate and hexane were distilled prior to usage. All moisture and oxygen sensitive reactions were performed under a nitrogen atmosphere (dried with Sicapent® from Merck and deoxygenated by a copper oxide catalyst R3-11 from BASF) using dry solvents obtained by a solvent purification system from Inert and degassed in a gentle stream of nitrogen for at least 10 min. Thin layer chromatography (TLC) was performed on pre-coated TLC sheets ALUGRAMR Xtra SIL G/UV254 from Macherey Nagel.

1.2. Nuclear Magnetic Resonance Spectroscopy

All NMR spectra were measured either at a Bruker Avance III HD 400 FT-Spectrometer (^{1}H: 400.13 MHz, ^{13}C: 100.61 MHz), with a Bruker Ultrashield Magnet, a Bruker Avance III HD 400 FT-Spectrometer (^{1}H: 400.03 MHz, ^{13}C: 100.59 MHz), with a Bruker Ascend Magnet or a Bruker Avance III HD 600 FT-Spectrometer (1H: 600.13 MHz, 13C: 150.90 MHz) equipped with a cryoprobe unit. Chemical shifts are given in ppm (δ-scale) referenced to the residual proton signal of the respective deuterated solvents (^{1}H) or to the signal of the present ^{13}C isotope. The proton signals and their coupling patterns are given as follows: s (singlet), d (doublet), dd (doublet of doublets), m (multiplet), AA' / BB' (chemically but not magnetically equivalent protons), m´ (overlapping signals of chemically non-equivalent protons that could not be assigned to first-order couplings). The carbon signals are given as: Cq (quaternary), CH (tertiary), CH_3 (primary).

1.3. Mass Spectrometry

Mass spectra were recorded on a Bruker Daltonic microTOF focus (ESI, APCI) or a Bruker Daltonics UltrafleXtreme (MALDI). For MALDI spectra DCTB (trans-2-[3-(4-*tert*-butylphenyl)-2-methyl-2- propenylidene]malononitrile) was used as a matrix. Respective theoretical masses were calculated using the software Bruker Daltonics Isotope Pattern. The given measured mass refers to the 100 % peak calculated by the software.

4-Bromo-*N*,*N*-bis(4-methoxyphenyl)aniline 3,4-anhydride-9,10-di(butylcarboxylate) perylene, *N*-(2,5-di-*tert*-butylphenyl)-9,10-di(butyl carboxylate) perylene monoimide, *N*-(2,5-di-*tert*-butylphenyl)-3,4-anhydride perylene monoimide and *N*-(2,5-di-*tert*-butylphenyl)-*N*'-(4-iodophenyl) perylene diimide were synthesised as *Mims et al.* reported.[1]

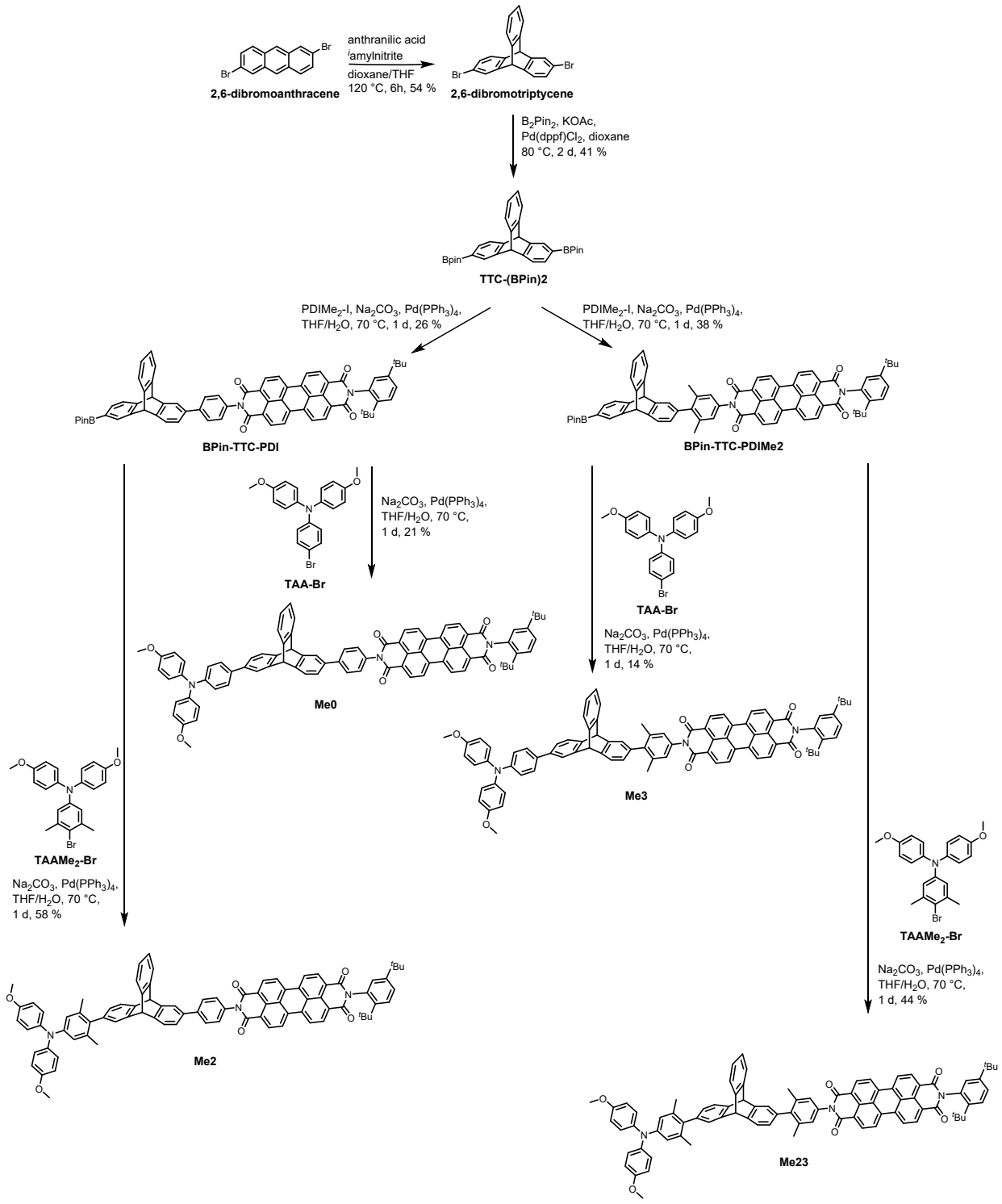
2,6-dibromoanthracene
anthranilic acid
isoamylnitrite
dioxane/THF
120 °C, 6h, 54 %
2,6-dibromotriptycene
B2Pin2, KOAc,
Pd(dppf)Cl2, dioxane
80 °C, 2 d, 41 %
TTC-(BPin)2
PDIMe2-I, Na2CO3, Pd(PPh3)4,
THF/H2O, 70 °C, 1 d, 26 %
PDIMe2-I, Na2CO3, Pd(PPh3)4,
THF/H2O, 70 °C, 1 d, 38 %
BPin-TTC-PDI
BPin-TTC-PDIMe2
TAA-Br
Na2CO3, Pd(PPh3)4,
THF/H2O, 70 °C,
1 d, 21 %
Me0
TAA-Br
Na2CO3, Pd(PPh3)4,
THF/H2O, 70 °C,
1 d, 14 %
Me3
TAAMe2-Br
Na2CO3, Pd(PPh3)4,
THF/H2O, 70 °C,
1 d, 58 %
Me2
TAAMe2-Br
Na2CO3, Pd(PPh3)4,
THF/H2O, 70 °C,
1 d, 44 %
Me23

Scheme S1

2,6-Dibromoanthracene

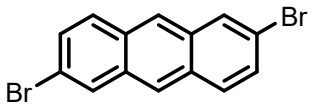

Synthesis according to literature.[2]

CAS: [186517-01-1]

2,6-Dibromoanthraquinone (3.00 g, 8.20 mmol) was suspended in acetic acid (170 ml) and stirred with hydrobromic acid (19.3 ml, 355 mmol, 48 % in H_2O) and phosphinic acid (14.5 ml, 265 mmol, 50 % in H_2O) for 5 d at 140 °C. The reaction mixture was poured into ice water and stirred for 30 min. The precipitate was filtered off and washed with water (2 x 50 ml), methanol (2 x 40 ml), toluene (3 x 20 ml) and was dried under vacuum.

Yield: 1.78 g (5.30 mmol, 65 %) of a yellow solid.

$C_{14}H_8Br_2$ [336.02 g/mol]

^{1}H-NMR (400.1 MHz, $CDCl_3$):

δ [ppm] = 8.33 (s, 2H), 8.19 (d, $^4J_{H,H}$ = 2.0 Hz, 2H), 7.90 (d, $^3J_{H,H}$ = 9.0 Hz, 2H), 7.56 (dd, $^3J_{H,H}$ = 9.1 Hz $^4J_{H,H}$ = 2.0 Hz, 2H).

Maldi-MS (pos): m/z calc. $[M]^{\cdot+}$ 335.90, found $[M]^{\cdot+}$ 335.98.

2,6-Dibromotriptycene

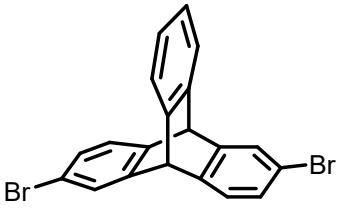

Synthesis according to literature.[3-5]

CAS: [186517-01-1]

2,6-Dibromoanthracene (1.00 g, 2.98 mmol) was dissolved in dry dioxane (70 ml) and heated to 120 °C. Anthranilic acid (816 mg, 5.95 mmol) was dissolved in dry THF (40 ml) and added dropwise to the anthracene solution via a syringe pump over 6 h. Isoamyl nitrite (6.00 ml, 44.6 mmol) was added simultaneously to the reaction mixture. After completed addition the mixture was stirred at 120 °C for further 30 min and afterwards cooled to r.t. The solvent was removed under reduced pressure and the product was separated from the reactant by washing the solid with hexanes/DCM (v:v 20:1 – 10:1). The crude product was purified by column chromatography (silica gel, hexanes/DCM 1:1, hexanes/tol 100:3).

Yield: 669 mg (1.62 mmol, 54 %) of a colourless solid.

$C_{20}H_{12}Br_2$ [412.12 g/mol]

^{1}H-NMR (400.1 MHz, $CDCl_3$):

δ [ppm] = 7.52 (d, $^4J_{H,H}$ = 1.9 Hz, 2H), 7.37 (m, 2H), 7.24 (d, $^3J_{H,H}$ = 7.8 Hz, 2H), 7.14 (dd, $^3J_{H,H}$ = 7.8 Hz, $^4J_{H,H}$ = 1.9 Hz, 2H), 7.02 (m, 2H), 5.35 (s, 2H).

APCI-DIP-MS (pos): m/z calc. $[M]^{\cdot+}$ 411.93, found $[M]^{\cdot+}$411.94.

2,6-Di(pinacolboron)triptycene (TTC-(Bpin)$_2$)

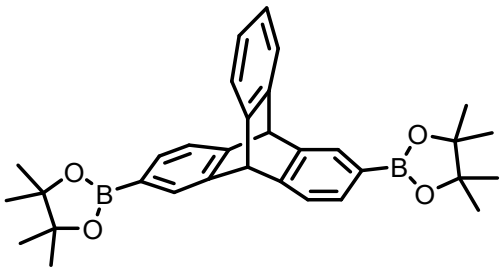

Synthesis according to literature.[6]

2,6-Dibromotriptycene (300 mg, 728 µmol), bis(pinacalto)diboron (462 mg, 1.82 mmol), Pd(dppf)Cl_2 (29.7 mg, 40.6 µmol) und potassium acetate (250 mg, 2.55 mmol) were dissolved in dry dioxane (25 ml) under nitrogen atmosphere. After stirring for 2 d at 80 °C the solvent was removed under reduced pressure and the residue was dissolved in DCM. The organic phase was washed with water (50 ml) and dried over $MgSO_4$. The solvent was removed under reduced pressure and the crude product was purified by column chromatography on silica gel (eluent: DCM/hexanes 3:2 – DCM).

Yield: 152 mg (300 µmol, 41 %) of a colourless solid.

$C_{32}H_{36}B_2O_4$ [506.25 g/mol]

^{1}H-NMR (400.1 MHz, $CDCl_3$):

δ [ppm] = 7.82 (m, 2H), 7.47 (dd, $^3J_{H,H}$ = 7.3 Hz, $^4J_{H,H}$ = 1.1 Hz, 2H), 7.37 (m, $^3J_{H,H}$ = 7.3 Hz, 2H), 7.34 (m, 2H), 6.96 (m, 2H), 5.44 (s, 2H), 1.30 (s, 24H).

^{13}C-NMR (100.6 MHz, $CDCl_3$):

δ [ppm] = 148.6 (C_q), 144.9 (C_q), 144.3 (C_q), 132.5 (CH), 129.7 (CH), 125.4 (CH), 123.8 (CH), 123.3 (CH), 83.8 (C_q), 54.2 (CH), 24.9 (CH_3).[1]

Maldi-MS (pos): m/z calc. $[M]^{\cdot+}$ 506.28, found $[M]^{\cdot+}$ 506.29.

[1] C-atom next to BPin is not visible.

***N*,*N*-Bis(4´-methoxyphenyl)-3,5-dimethylaniline**

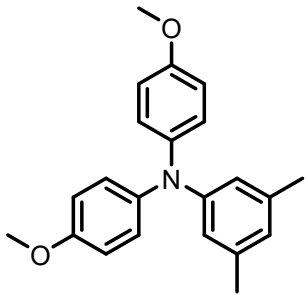

Synthesis according to literature.[7]

CAS: [220093-15-4]

3,5-Dimethylaniline (3.00 g, 24.8 mmol) 4-iodoanisole (12.8 g, 54.7 mmol), copper(I)-iodide (377 mg, 1.98 mmol), 1,10-phenanthroline (357 mg, 1.98 mmol) and potassium hydroxide (3.61 g, 64.3 mmol) were suspended in dry toluene (50 ml) under nitrogen atmosphere. The reaction mixture was heated to 110 °C for 3 d. The solvent was removed under reduced pressure and the residue was dissolved with DCM. The organic phase was washed with water (60 ml) and the solvent was removed under reduced pressure. The crude product was purified by column chromatography on silica gel (eluent: DCM/hexanes 3:2). The crude solid was dissolved in DCM and precipitated from MeOH at -30 °C.

Yield: 990 mg (2.97 mmol, 12 %) of a colourless solid.

$C_{22}H_{23}NO_2$ [333.42 g/mol]

^{1}H-NMR (400.1 MHz, acetone-d_6):

δ [ppm] = 6.88 (AA´, 4H), 6.86 (BB´, 4H), 6.52 (m, 1H), 6.50 (m, 2H), 3.78 (s, 6H), 2.15 (s, 6H).

Maldi-MS (pos): m/z calc. $[M]^{\cdot+}$ 333.17, found $[M]^{\cdot+}$ 333.17.

4-Bromo-*N*,*N*-bis(4-methoxyphenyl)3,5-dimethylaniline

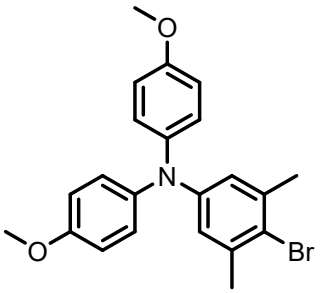

Synthesis according to literature.[7]

CAS: [220093-24-5]

N,*N*-Bis(4´-methoxyphenyl)-3,5-dimethylaniline (200 mg, 600 µmol) was dissolved in EtOAc (20 ml) and was cooled to 0 °C. *N*-Bromosuccimide (107 mg, 601 µmol) was added within 1 h, afterwards the reaction mixture was warmed up to r.t. and stirred for 1 d under light exclusion. The organic layer was washed with brine (50 ml) and dried over $MgSO_4$. The crude product was dissolved in DCM, put in an access of MeOH and precipitated at -30 °C.

Yield: 174 mg (422 µmol, 70 %) of a colourless solid.

$C_{22}H_{22}BrNO_2$ [412.32 g/mol]

^{1}H-NMR (400.1 MHz, acetone-d_6):

δ [ppm] = 7.02 (AA´, 4H), 6.90 (BB´, 4H), 6.64 (m, 2H), 3.78 (s, 6H), 2.24 (s, 6H).

Maldi-MS (pos): m/z calc. $[M]^{\cdot+}$ 413.08, found $[M]^{\cdot+}$ 413.08.

***N*-(2,5-Di-*tert*-butylphenyl)-*N'*-(4-iodo-3,5-dimethylphenyl) perylene diimide**

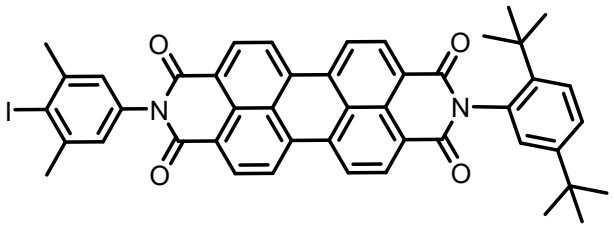

Synthesis according to literature.[1]

N-(2,5-Di-*tert*-butylphenyl)-3,4-anhydride perylene monoimide (1.00 g, 1.73 mmol) 4-iodo-3,5-dimethylaniline (853 mg, 3.45 mmol) and $ZnOAc \cdot 2H_2O$ (189 mg, 861 µmol) were added to 1*H*-imidazole (15 g) under a nitrogen atmosphere, heated to 140 °C and stirred for 5 h. After cooling aqueous HCl (2 M) was added and stirred until all 1*H*-imidazole was dissolved. The red solid was filtered off, washed with water and dried *in vacuo*. The crude product was purified by column chromatography on silica gel (eluent: CH_2Cl_2 – CH_2Cl_2 containing 1% EtOAc).

Yield: 1.26 g (1.56 mmol, 90 %) of a red solid.

$C_{46}H_{37}IN_2O_4$ [808.70 g/mol]

^{1}H-NMR (400.1 MHz, $CDCl_3$):

δ [ppm] = 8.75 (m´, 8H), 7.61 (d, $^3J_{H,H}$ = 8.6 Hz, 1H), 7.48 (dd, $^3J_{H,H}$ = 8.6 Hz, $^4J_{H,H}$ = 2.3 Hz, 1H), 7.08 (s, 2H), 7.05 (d, $^4J_{H,H}$ = 2.3 Hz, 1H), 2.56 (s, 6H), 1.33 (s, 9H), 1.29 (s, 9H).

^{13}C-NMR (100.6 MHz, $CDCl_3$):

δ [ppm] = . 164.4 (C_q), 163.6 (C_q), 150.4 (C_q), 143.8 (C_q), 143.7 (C_q), 135.2 (C_q), 134.8 (C_q), 134.6 (C_q), 132.6 (C_q), 131.95 (CH), 131.93 (CH), 129.9 (C_q), 129.8 (C_q), 128.9 (CH), 128.0 (CH), 126.9 (CH), 126.8 (C_q), 126.7 (C_q), 126.5 (CH), 124.0 (C_q), 123.5 (CH), 123.4 (CH), 123.3 (C_q), 109.4 (C_q), 35.7 (C_q), 34.4 (C_q), 31.9 (CH_3), 31.3 (CH_3), 29.9 (CH_3).

APCI-MS (pos): m/z calc. $[M+H]^{\cdot+\cdot}$ 809.19, found $[M+H]^{\cdot+\cdot}$ 809.18.

(Bpin)-TTC-PDI-Me$_2$

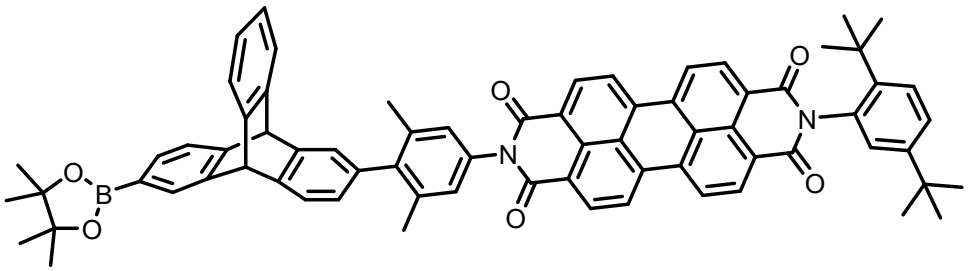

Synthesis according to literature.[6]

TTC-(Bpin)$_2$ (100 mg, 198 µmol), **PDI-Me$_2$-I** (80.5 mg, 99.5 µmol) and sodium carbonate (39.8 mg, 376 µmol) were dissolved in a mixture of dry THF (6 ml) and degassed water (1.5 ml) under a nitrogen atmosphere. Afterwards $Pd(PPh_3)_4$ (5.42 mg, 4.69 µmol) was added and the reaction mixture heated to 70 °C for 1 d. The solvent was removed under reduced pressure, the residue dissolved in DCM and the organic layer washed three times with water (30 ml). The aqueous layers were extracted with DCM (70 ml) and the combined organic layers were dried over Na_2SO_4.The solvent was removed under reduced pressure and the crude product was purified by column chromatography on silica gel (eluent: DCM – DCM/tol (5:1) – DCM/tol/EA (500:100:3).

Yield: 40.0 mg (37.7 µmol, 38 %) of a red solid.

$C_{72}H_{61}BN_2O_6$ [1061.08 g/mol]

^{1}H-NMR (400.1 MHz, $CDCl_3$):

δ [ppm] = 8.75 (m', 8H), 7.88 (s, 2H), 7.61 (d, $^3J_{H,H}$ = 7.3 Hz, 1H), 7.52 (dd, $^3J_{H,H}$ = 7.3 Hz, $^4J_{H,H}$ = 1.1 Hz, 1H), 7.48 (dd, $^3J_{H,H}$ = 8.6 Hz, $^4J_{H,H}$ = 2.3 Hz, 1H), 7.43 (m', 4H), 7.25 (d, $^4J_{H,H}$ = 1.5 Hz, 1H), 7.02 (m', 5H), 6.85 (dd, $^3J_{H,H}$ = 7.5 Hz, $^4J_{H,H}$ = 1.6 Hz, 1H), 5.49 (s, 1H), 5.46 (s, 1H), 2.00 (s, 3H), 1.98 (s, 3H), 1.34 (s, 9H), 1.31 (s, 12H), 1.30 (s, 12H).

^{13}C-NMR (100.6 MHz, $CDCl_3$):

δ [ppm] = .164.6 (C_q), 163.9. (C_q), 150.3. (C_q), 149.0 (C_q), 145.5 (C_q), 145.22 (C_q), 145.20 (C_q), 145.0 (C_q), 143.9 (C_q), 143.8 (C_q), 142.5 (C_q), 138.21 (C_q), 138.15 (C_q), 137.4 (C_q), 135.2 (C_q), 135.1 (C_q), 133.5 (C_q), 132.7 (C_q), 132.4 (CH), 132.12 (CH), 132.07 (CH), 130.1 (C_q), 129.3

(C_q), 129.6 (CH), 129.0 (CH), 127.8 (CH), 127.0 (2 x CH), 126.9 (2 x C_q), 126.6 (CH), 126.0 (CH), 125.4 (CH), 125.3 (CH), 124.4 (CH), 123.93 (CH), 123.89 (C_q), 123.8 (2 x CH), 123.7 (C_q), 123.51 (CH), 123.48 (CH), 123.40 (CH), 83.9 (C_q), 54.5 (CH), 54.0 (CH), 35.7 (C_q), 34.5 (C_q), 31.9 (CH_3), 31.4 (CH_3), 25.0 (CH_3), 21.43 (CH_3),21.41 (CH_3).[2]

ESI-HRMS (pos): m/z calc. $[M+Na]^{\cdot+}$ 1083.45264, found $[M+Na]^{\cdot+}$ 1083.45149, Δ = 1.06 ppm.

(Bpin)-TTC-PDI

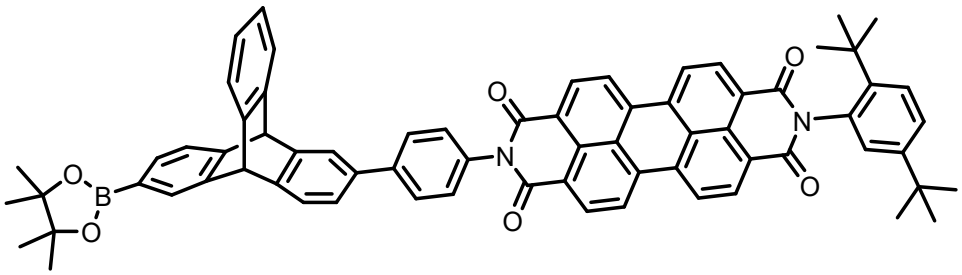

Synthesis according to literature.[6]

TTC-(Bpin)$_2$ (463 mg, 915 µmol), **PDI-I** (357 mg, 457 µmol) and sodium carbonate (194 mg, 1.83 mmol) were dissolved in a mixture of dry THF (12 ml) and degassed water (3 ml) under a nitrogen atmosphere. Afterwards $Pd(PPh_3)_4$ (26.4 mg, 22.8 µmol) was added and the reaction mixture heated to 70 °C for 1 d. The solvent was removed under reduced pressure, the residue dissolved in DCM and the organic layer washed three times with water (30 ml). The aqueous layers were extracted with DCM (70 ml) and the combined organic layers were dried over Na_2SO_4.The solvent was removed under reduced pressure and the crude product was purified by column chromatography on silica gel (eluent: DCM – DCM/tol (5:1) – DCM/tol/EA (500:100:3)).

Yield: 123 mg (119 µmol, 26 %) of a red solid.

$C_{70}H_{57}BN_2O_6$ [1033.03 g/mol]

^{1}H-NMR (400.1 MHz, $CDCl_3$):

[2] C-atom next to BPin unit is not visible.

δ [ppm] = 8.77 (m', 8H), 7.88 (s, 1H), 7.69 (m', 3H), 7.61 (d, $^{3}J_{H,H}$ = 8.6 Hz, 1H), 7.52 (dd, $^{3}J_{H,H}$ = 7.3 Hz, $^{4}J_{H,H}$ = 1.1 Hz, 1H), 7.43 (m', 7H), 7.26 (m', 1H), 7.02 (m', 3H), 5.53 (s, 1H), 5.51 (s, 1H), 1.33 (s, 9H), 1.31 (s, 12H), 1.30 (s, 9H).

^{13}C-NMR (100.6 MHz, $CDCl_3$):

δ [ppm] = 164.6 (C_q), 163.8. (C_q), 150.4. (C_q), 148.6. (C_q), 145.7. (C_q), 145.1. (C_q), 144.83. (C_q), 144.81. (C_q), 144.6. (C_q), 143.9. (C_q), 142.3. (C_q), 137.9. (C_q), 135.3. (C_q), 135.1. (C_q), 134.0. (C_q), 132.7. (C_q), 132.6 (CH), 132.1 (CH, 2C), 130.1. (C_q), 130.0. (C_q), 129.7 (CH), 129.0 (CH), 128.9 (CH), 128.5 (CH), 127.8 (CH), 127.0. (C_q), 126.9. (C_q), 126.6 (CH), 125.6 (CH), 125.4 (CH), 124.6 (CH), 124.1 (CH), 124.0 (CH), 123.9. (C_q), 123.8 (CH), 123.6. (C_q), 123.54 (CH), 123.47 (CH), 123.42 (CH), 123.1 (CH), 83.8. (C_q), 54.6 (CH), 53.8 (CH), 35.7. (C_q), 34.2. (C_q), 31.9 (CH_3), 31.4 (CH_3), 24.9 (CH_3).[3]

ESI-HRMS (pos): m/z calc. $[M+Na]^+$ 1055.42131, found $[M+Na]^+$ 1055.41985; Δ = 1.38 ppm.

Me2Me$_2$ = Me23

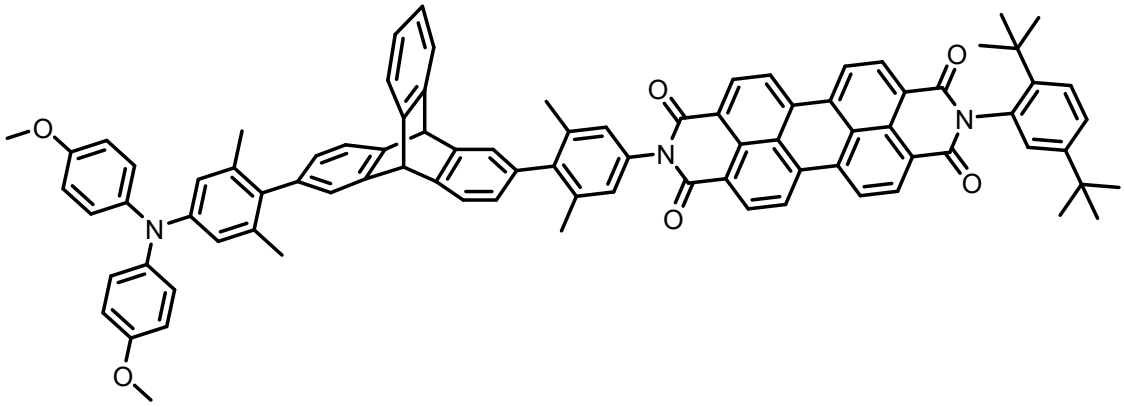

Synthesis according to literature.[6]

Bpin-TTC-PDI-Me$_2$ (23.0 mg, 21.7 µmol), **TAA-Me$_2$-Br** (13.4 mg, 32.5 µmol) and sodium carbonate (9.17 mg, 86.5 µmol) were dissolved in a mixture of dry THF (12 ml) and degassed water (3 ml) under a nitrogen atmosphere. Afterwards $Pd(PPh_3)_4$ (1.25 mg, 10.8 µmol) was added and the reaction mixture heated to 70 °C for 1 d. The solvent was removed under reduced pressure, the residue dissolved in DCM and the organic layer washed three times with water (20 ml). The aqueous layers were extracted with DCM (30 ml) and the combined

[3] C-atom next to BPin unit is not visible.

organic layers were dried over Na_2SO_4. The solvent was removed under reduced pressure and the crude product was purified twice by column chromatography on silica gel (eluent: DCM containing 1 % of EA; Tol/EA 7:1). The product was dissolved in DCM and precipitated by addition of hexane.

Yield: 12.0 mg (9.47 µmol, 44 %) of a red solid.

$C_{88}H_{71}N_3O_6$ [1266.53 g/mol]

^{1}H-NMR (600.1 MHz, CD_2Cl_2):

δ [ppm] = 8.76 (m', 8H), 7.63 (d, $^3J_{H,H}$ = 8.7 Hz, 1H), 7.54 (d, $^3J_{H,H}$ = 8.7 Hz, 1H), 7.51 (dd, $^3J_{H,H}$ = 8.7 Hz, $^4J_{H,H}$ = 2.3 Hz, 1H), 7.49 (d, $^3J_{H,H}$ = 7.6 Hz, 1H), 7.47 (m', 2H), 7.37 (d, $^4J_{H,H}$ = 1.5 Hz, 1H), 7.26 (d, $^4J_{H,H}$ = 1.6 Hz, 1H), 7.06 (m', 5H), 7.04 (AA', 4H), 6.96 (dd, $^3J_{H,H}$ = 7.3 Hz, $^4J_{H,H}$ = 1.6 Hz, 1H), 6.83 (m', 5H), 6.63 (m, 2H), 5.55 (s, 1H), 5.53 (s, 1H), 3.78 (s, 6H), 2.09 (s, 3H), 2.04 (s, 3H), 1.88 (s, 3H), 1.82 (s,3H), 1.34 (s, 9H), 1.28 (s, 9H).

^{13}C-NMR (150.9 MHz, CD_2Cl_2):

δ [ppm] = .164.9 (C_q), 164.1 (C_q), 156.1 (C_q), 150.8(C_q), 147.7 (C_q), 146.3 (C_q), 146.2 (C_q), 145.8 (C_q), 144.8 (C_q), 144.5 (C_q), 143.8 (C_q), 142.6 (C_q), 141.6 (C_q), 139.7 (C_q), 138.5 (C_q), 138.24 (C_q), 138.15 (C_q), 137.6 (C_q), 137.2 (C_q), 137.1 (C_q), 135.5 (C_q), 135.4 (C_q), 134.8 (C_q), 134.5 (C_q), 133.6 (C_q), 132.1 (CH), 132.0 (CH), 130.3 (C_q), 130.2 (C_q), 129.3 (CH), 128.3 (CH), 127.6 (CH), 127.23 (C_q), 127.15 (C_q), 126.9 (2 x CH) 126.8 (CH), 126.6 (CH), 126.5 (CH), 126.3 (CH), 125.5 (CH), 125.4 (CH), 142.7 (CH) 124.2 (CH), 124.07 (CH), 124.06 (C_q), 124.02 (CH), 123.97 (CH), 123.89 (CH), 123.88 (C_q), 123.87 (CH), 120.1 (2 x CH), 114.9 (CH), 55.8 (CH_3), 54.2 (CH), 54.1 (CH), 35.8 (C_q), 35.6 (C_q), 31.8 (CH_3), 13.3 (CH_3), 21.29 (CH_3), 21.27 (CH_3), 21.25 (CH_3), 21.23 (CH_3).

ESI-HRMS (pos): m/z calc. $[M]^{\cdot+}$ 1265.53374, found $[M]^{\cdot+}$ 1265.53712, Δ = 2.67 ppm.

TAAMe$_2$-TTC-PDI = Me2

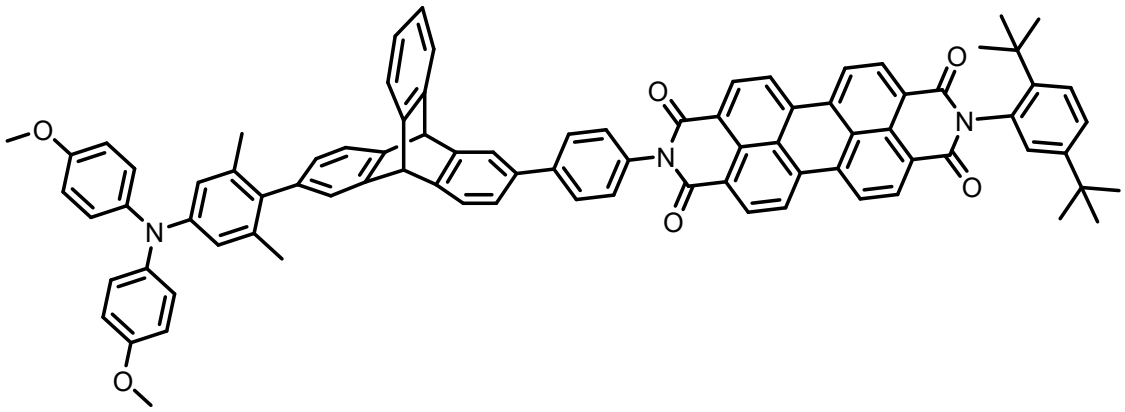

Synthesis according to literature.[6]

Bpin-TTC-PDI (36.0 mg, 34.8 µmol), **TAA-Me$_2$-Br** (28.7 mg, 69.6 µmol) and sodium carbonate (14.7 mg, 139 µmol) were dissolved in a mixture of dry THF (6 ml) and degassed water (1.5 ml) under a nitrogen atmosphere. Afterwards, $Pd(PPh_3)_4$ (2.01 mg, 1.74 µmol) was added and the reaction mixture heated to 70 °C for 1 d. The solvent was removed under reduced pressure, the residue dissolved in DCM and the organic layer washed three times with water (20 ml). The aqueous layers were extracted with DCM (30 ml) and the combined organic layers were dried over Na_2SO_4.The solvent was removed under reduced pressure and the crude product was purified by column chromatography (eluent: DCM). The product was dissolved in DCM and precipitated by addition of hexane.

Yield: 25.0 mg (20.2 µmol, 58 %) of a red solid.

$C_{86}H_{67}N_3O_6$ [1238.47 g/mol]

^{1}H-NMR (600.1 MHz, CD_2Cl_2):

δ [ppm] = 8.75 (m', 8H), 7.77 (d, $^4J_{H,H}$ = 1.8 Hz, 1H), 7.75 (AA', 2H), 7.62 (d, $^3J_{H,H}$ = 8.7 Hz, 1H), 7.54 (d, $^3J_{H,H}$ = 7.7 Hz, 1H), 7.51 (m', 2H), 7.49 (m', 1H), 7.45 (m', 1H), 7.40 (BB', 2H), 7.36 (dd, $^3J_{H,H}$ = 7.7 Hz, $^4J_{H,H}$ = 1.8 Hz, 1H), 7.25 (d, $^4J_{H,H}$ = 1.7 Hz, 1H), 7.07 (m', 3H), 7.04 (AA', 4H), 6.83 (m', 5H), 6.62 (s, 2H), 5.60 (s, 1H), 5.53 (s, 1H), 3.78 (s, 6H), 1.84 (s, 3H), 1.82 (s, 3H), 1.33 (s, 9H), 1.28 (s, 9H).

^{13}C-NMR (150.9 MHz, CD_2Cl_2):

δ [ppm] = 164.9 (C_q), 164.0 (C_q), 156.1 (C_q), 150.8 (C_q), 147.7 (C_q), 146.8 (C_q), 145.84 (C_q), 145.81 (C_q), 145.6 (C_q), 145.5(C_q), 144.6 (C_q), 143.5 (C_q), 142.1 (C_q), 141.6 (C_q), 138.6 (C_q), 138.0 (C_q), 137.16 (C_q), 137.15 (C_q), 135.5 (C_q), 135.4 (C_q), 134.9 (C_q), 134.8 (C_q), 133.6 (C_q), 132.1 (CH), 132.0 (CH), 130.24 (C_q), 130.16 (C_q),129.4 (CH),129.3 (CH),128.4 (CH), 128.3 (CH), 127.2 (C_q),127.1 (C_q),127.0 (CH), 126.8 (CH), 2C), 126.5 (CH), 125.7 (CH), 125.6 (CH), 125.4 (CH), 124.7 (CH), 124.4 (CH), 124.09 (C_q), 124.08 (CH, 2C), 124.0 (CH), 123.9 (C_q), 123.89 (CH), 123.88 (CH), 123.2 (CH), 120.1 (CH), 114.9 (CH), 55.8 (CH_3), 54.22 (CH), 54.18 (CH), 35.8 (C_q), 35.6 (C_q), 31.8 (CH_3), 31.3 (CH_3), 21.31 (CH_3), 21.27 (CH_3).

ESI-HRMS (pos): m/z calc. $[M]^{\cdot+}$ 1237.50244, found $[M]^{\cdot+}$ 1237.50133, Δ = 0.90 ppm.

TAA-TTC-PDIMe$_2$ = Me3

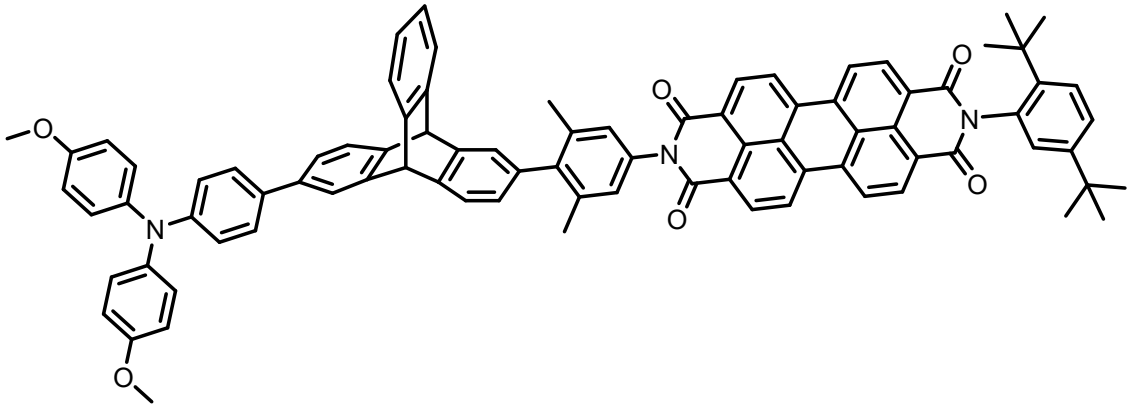

Synthesis according to literature.[6]

Bpin-TTC-PDI-Me$_2$ (73.0 mg, 68.7 µmol), **TAA-Br** (52.8 mg, 137 µmol) and sodium carbonate (29.1 mg, 275 µmol) were dissolved in a mixture of dry THF (12 ml) and degassed water (3 ml) under a nitrogen atmosphere. Afterwards, $Pd(PPh_3)_4$ (3.97 mg, 3.43 µmol) was added and the reaction mixture heated to 70 °C for 1 d. The solvent was removed under reduced pressure, the residue dissolved in DCM and the organic layer washed three times with water (20 ml). The aqueous layers were extracted with DCM (30 ml) and the combined organic layers were dried over Na_2SO_4.The solvent was removed under reduced pressure and the crude product was purified by column chromatography (eluent: DCM). The product was dissolved in DCM and precipitated by addition of hexane.

Yield: 12.0 mg (9.69 µmol, 14 %) of a red solid.

$C_{86}H_{67}N_3O_6$ [1238.47 g/mol]

^{1}H-NMR (600.1 MHz, CD_2Cl_2):

δ [ppm] = 8.76 (m', 8H), 7.65 (d, $^4J_{H,H}$ = 1.7 Hz, 1H), 7.63 (d, $^3J_{H,H}$ = 8.7 Hz, 1H), 7.55 (d, $^3J_{H,H}$ = 7.4 Hz, 1H), 7.51 (dd, $^3J_{H,H}$ = 8.7 Hz, $^4J_{H,H}$ = 2.2 Hz, 1H), 7.47 (m', 3H), 7.38 (AA', 2H), 7.35 (d, $^4J_{H,H}$ = 1.5 Hz, 1H), 7.21 (dd, $^3J_{H,H}$ = 7.7 Hz, $^4J_{H,H}$ = 1.7 Hz, 1H), 7.06 (m', 9H), 6.95 (dd, $^3J_{H,H}$ = 7.4 Hz, $^4J_{H,H}$ = 1.6 Hz, 1H), 6.93 (BB', 2H), 6.84 (BB', 4H), 5.57 (s, 1H), 5.53 (s, 1H), 3.78 (s, 6H), 2.05 (s, 3H), 2.04 (s, 3H), 1.34 (s, 9H), 1.27 (s, 9H).

^{13}C-NMR (150.9 MHz, CD_2Cl_2):

δ [ppm] = .164.9 (C_q), 164.1 (C_q), 156.5 (C_q), 150.8 (C_q), 148.5 (C_q), 146.4 (C_q), 146.0(C_q), 145.4 (C_q), 145.8 (C_q), 144.6 (C_q), 144.3 (C_q), 144.2 (C_q), 142.6 (C_q), 141.2 (C_q), 138.5 (C_q), 138.19 (C_q), 138.18 (C_q), 137.7 (C_q), 135.5 (C_q), 135.4 (C_q), 134.5 (C_q), 133.6 (C_q), 133.2 (C_q), 132.1 (CH), 132.0 (CH), 130.3 (C_q), 130.2 (C_q), 129.3 (CH), 128.3 (CH), 127.8 (CH, 2C), 127.6 (CH), 127.24 (C_q), 127.16 (C_q), 127.1 (CH), 126.6 (CH), 126.4 (CH), 125.7 (CH), 125.6 (CH), 124.7 (CH), 124.3 (CH), 124.2 (CH) 124.08 (CH), 124.05 (C_q), 124.04 (CH), 124.02 (C_q), 123.9 (CH), 123.87 (CH), 123.6 (CH), 122.4 (CH), 120.8 (CH), 115.0 (CH), 55.8 (CH_3), 54.3 (CH), 54.0 (CH), 35.8 (C_q), 35.6 (C_q), 31.8 (CH_3), 31.4 (CH_3), 21.3 (CH_3), 21.2 (CH_3).

ESI-HRMS (pos): m/z calc. $[M]^{\cdot+}$ 1237.50244, found $[M]^{\cdot+}$ 1237.49840, Δ = 3.62 ppm.

TAA-TTC-PDI = Me0

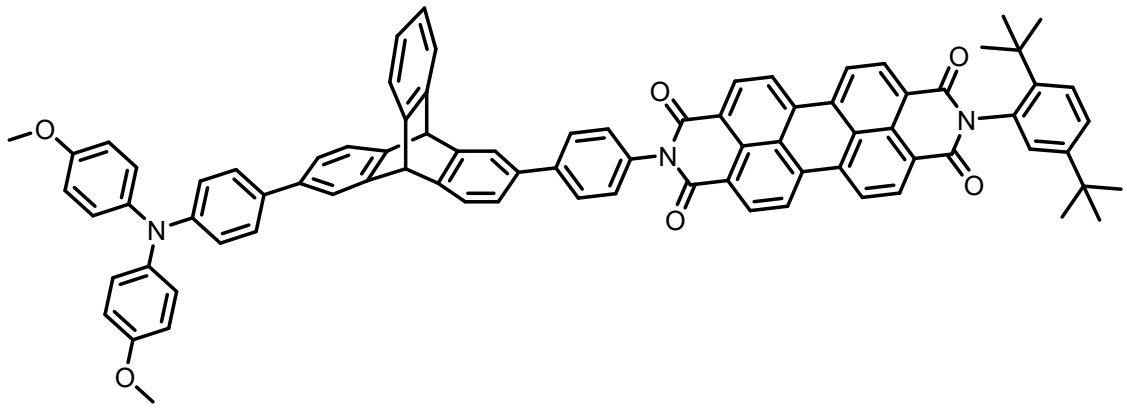

Synthesis according to literature.[6]

Bpin-TTC-PDI (123 mg, 119 µmol), **TAA-Br** (91.3 mg, 238 µmol) and sodium carbonate (50.4 mg, 476 µmol) were dissolved in a mixture of dry THF (12 ml) and degassed water (3 ml) under a nitrogen atmosphere. Afterwards $Pd(PPh_3)_4$ (6.87 mg, 5.95 µmol) was added and the reaction mixture heated to 70 °C for 1 d. The solvent was removed under reduced pressure, the residue dissolved in DCM and the organic layer washed three times with water (20 ml). The aqueous layers were extracted with DCM (30 ml) and the combined organic layers were dried over Na_2SO_4.The solvent was removed under reduced pressure and the crude product was purified by column chromatography (eluent: DCM; DCM/tol/EA 400:100:4). The product was dissolved in DCM and precipitated by addition of hexane.

Yield: 30.0 mg (24.8 µmol, 21 %) of a red solid.

$C_{84}H_{63}N_3O_6$ [1210.42 g/mol]

^{1}H-NMR (600.1 MHz, CD_2Cl_2):

δ [ppm] = 8.74 (m', 8H), 7.75 (d, $^4J_{H,H}$ = 1.7 Hz, 1H), 7.73 (AA', 2H), 7.64 (d, $^4J_{H,H}$ = 1.8 Hz, 1H), 7.62 (d, $^3J_{H,H}$ = 8.7 Hz, 1H), 7.45 (d, $^3J_{H,H}$ = 7.6 Hz, 1H), 7.51 (dd, $^3J_{H,H}$ = 8.7 Hz, $^4J_{H,H}$ = 2.2 Hz, 1H), 7.48 (m', 3H), 7.40 (BB', 2H) 7.36 (m', 3H), 7.21 (dd, $^3J_{H,H}$ = 7.7 Hz, $^4J_{H,H}$ = 1.8 Hz, 1H), 7.08 (d, $^4J_{H,H}$ = 2.2 Hz, 1H), 7.06 (m' ,6H), 6.92 (BB', 2H), 6.84 (BB', 4H), 5.58 (s, 1H), 5.57 (s, 1H), 3.78 (s, 6H), 1.33 (s, 9H), 1.28 (s, 9H).

^{13}C-NMR (150.9 MHz, CD_2Cl_2):

δ [ppm] = .164.8 (C_q), 164.0 (C_q), 156.5 (C_q), 150.8 (C_q), 148.5 (C_q), 146.5 (C_q), 146.1 (C_q), 145.52 (C_q), 145.45 (C_q), 145.3 (C_q), 144.6 (C_q), 143.8 (C_q), 142.1 (C_q), 141.2 (C_q), 138.7 (C_q), 138.1 (C_q), 135.5 (C_q), 135.4 (C_q), 134.9 (C_q), 133.6 (C_q), 133.2 (C_q), 132.1 (CH), 132.0 (CH), 130.23 (C_q), 130.15 (C_q), 129.4 (CH), 129.3 (CH), 128.4 (CH), 128.3 (CH), 127.8 (CH), 127.2 (C_q), 127.12 (C_q), 127.07 (CH), 126.5 (CH), 125.8 (CH), 125.7 (CH), 124.8 (CH), 124.4 (CH), 124.3 (CH), 124.081 (2 x CH), 124.077 (C_q), 123.89 (2 x CH), 123.88 (C_q), 123.7 (CH), 123.1 (CH), 122.4 (CH), 120.8 (CH), 115.0 (CH), 55.8 (CH_3), 54:1 (CH); 54:0 (CH); 35.8 (C_q), 34.6 (C_q), 31.8 (CH_3), 31.3 (CH_3).

ESI-HRMS (pos): m/z calc. $[M]^{\cdot+}$ 1209.47114, found $[M]^{\cdot+}$ 1209.47015, Δ = 0.82 ppm.

1.4. NMR spectra of all triads and precursors

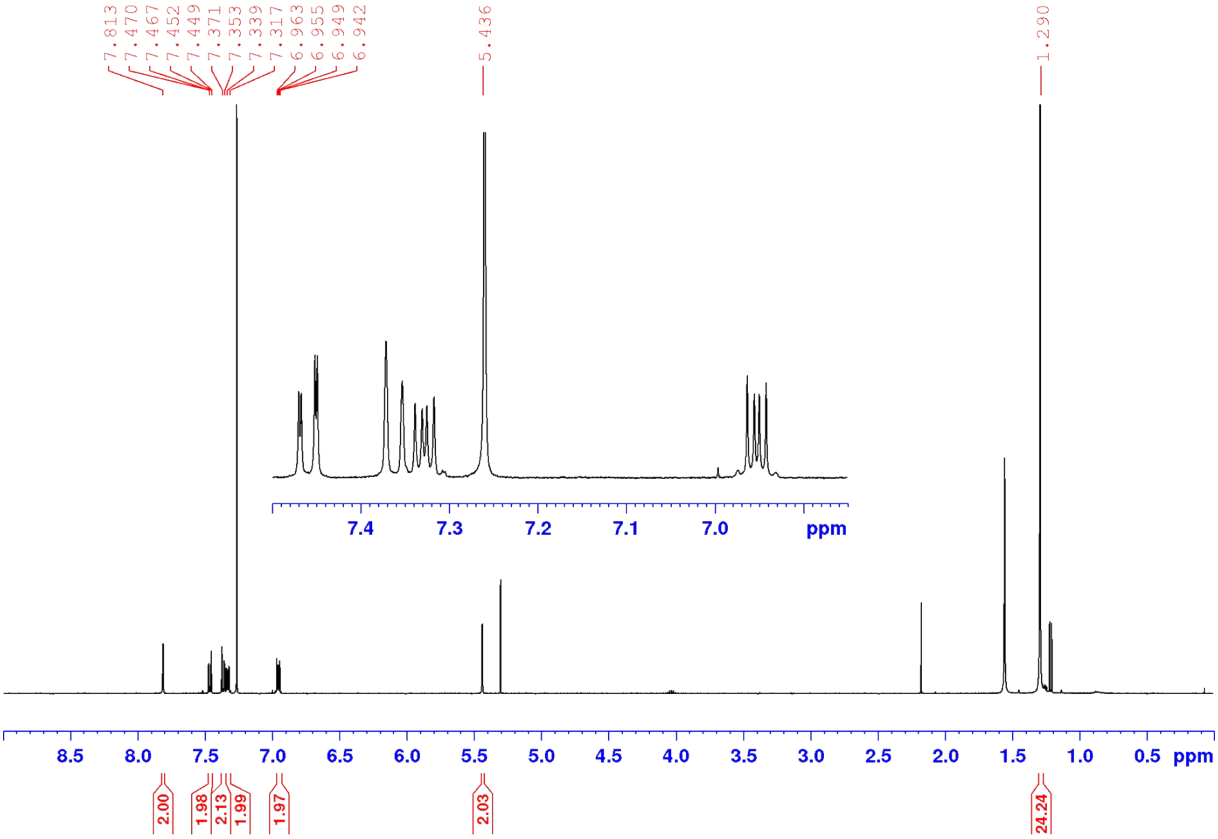

Fig. S1 ^{1}H-NMR: TTC-$(BPin)_2$ ($CDCl_3$, 400.1 MHz).

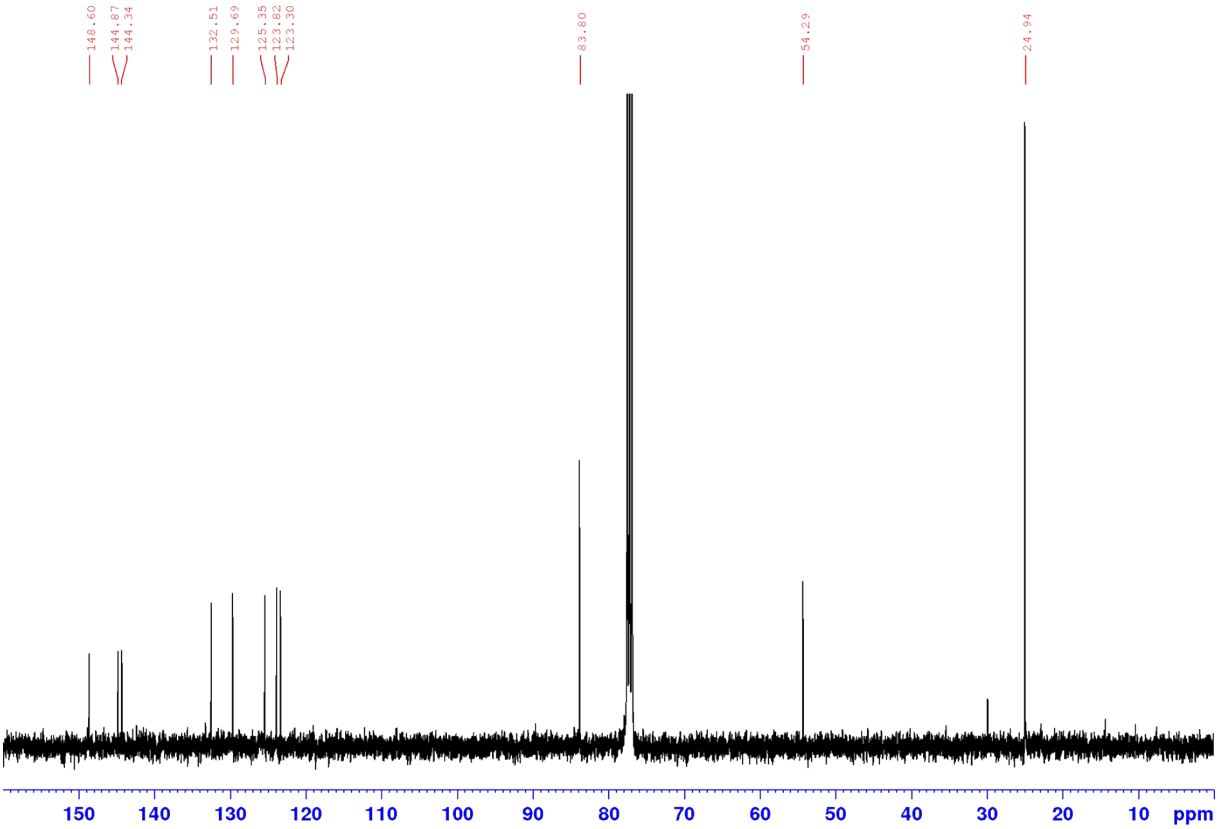

Fig. S2 ^{13}C-NMR: TTC-$(BPin)_2$ ($CDCl_3$, 100.6 MHZ).

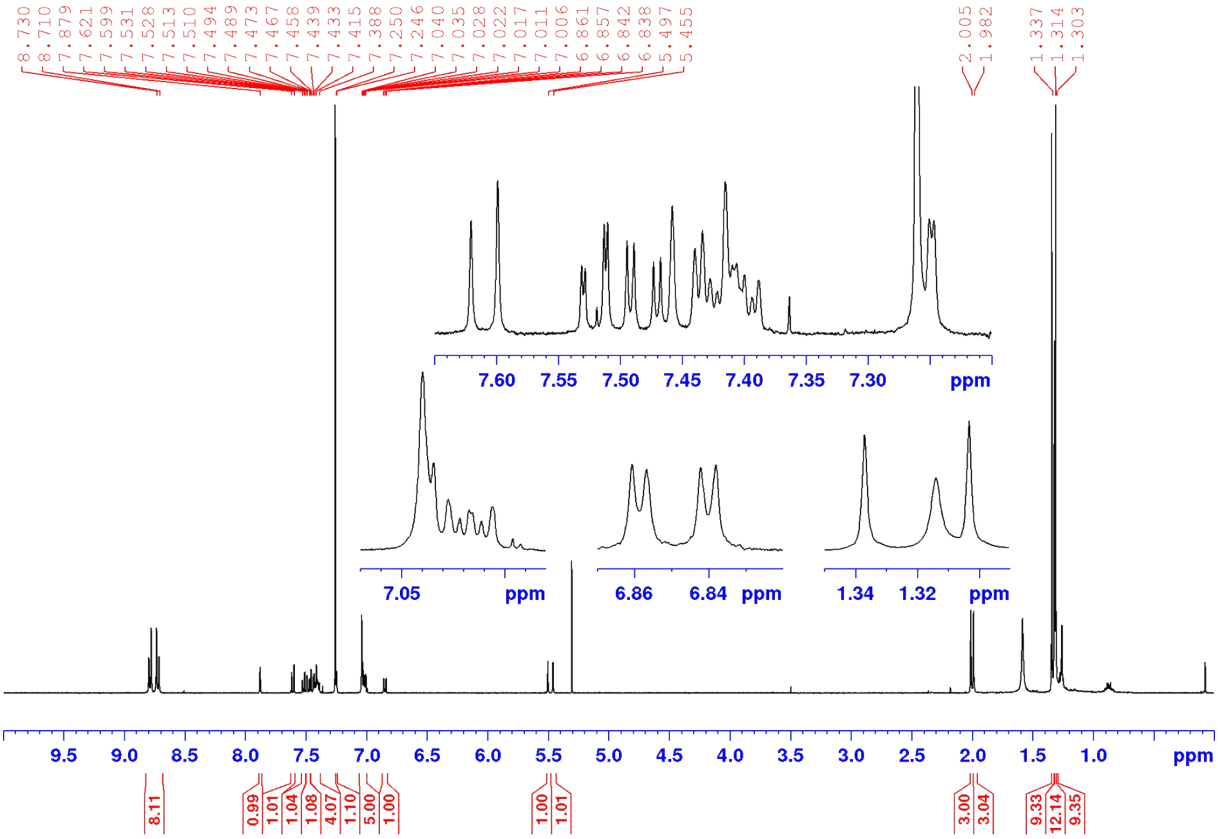

Fig. S3 ^{1}H-NMR: BPin-TTC-PDIMe$_2$ ($CDCl_3$, 400.1 MHz).

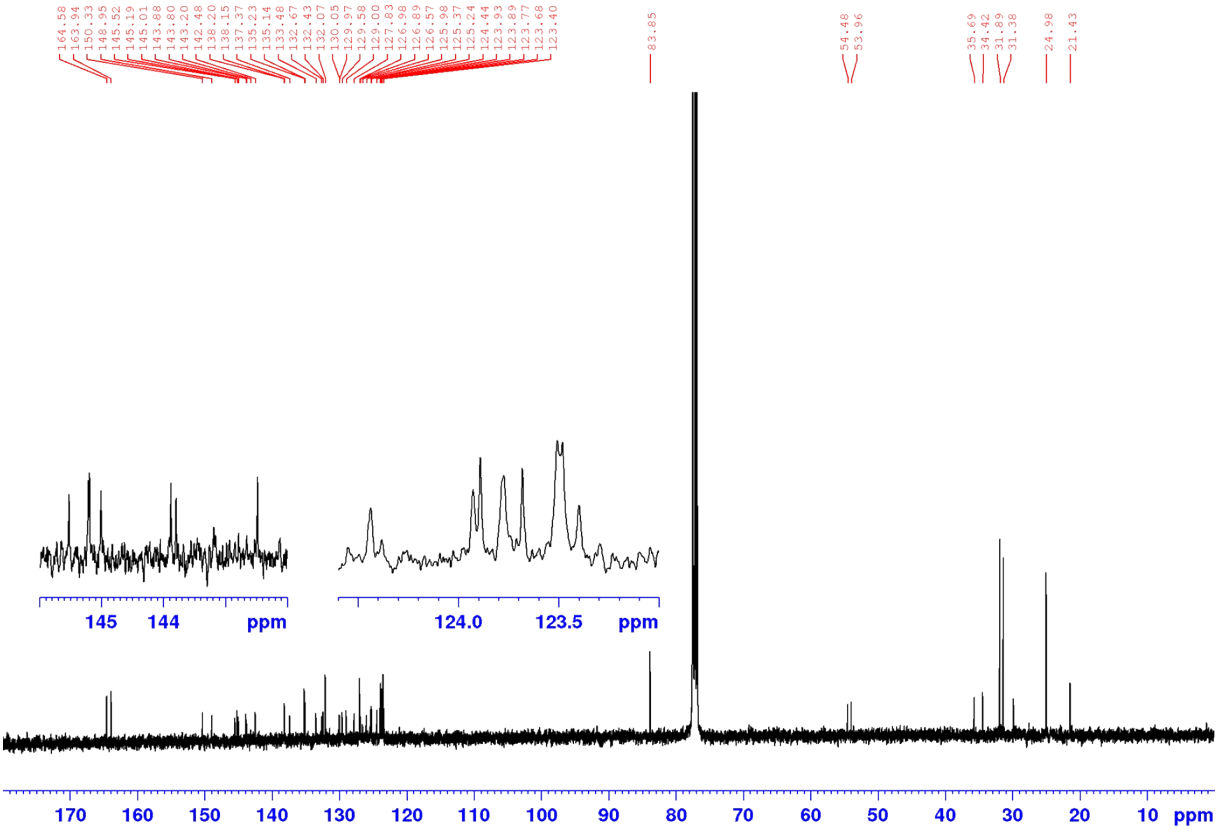

Fig. S4 ^{13}C-NMR: BPin-TTC-PDIMe$_2$ ($CDCl_3$, 100.6 MHZ).

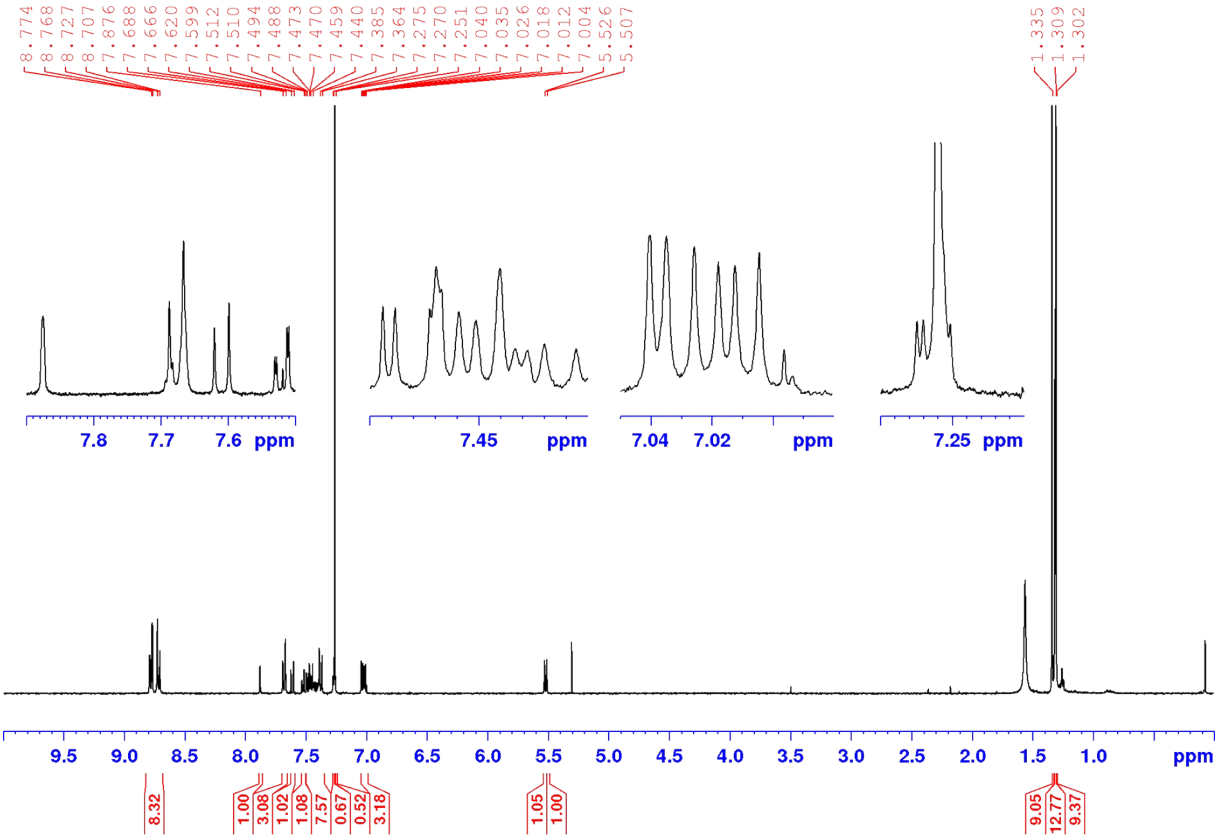

Fig. S5 ^{1}H-NMR: BPin-TTC-PDI ($CDCl_3$, 400.1 MHz).

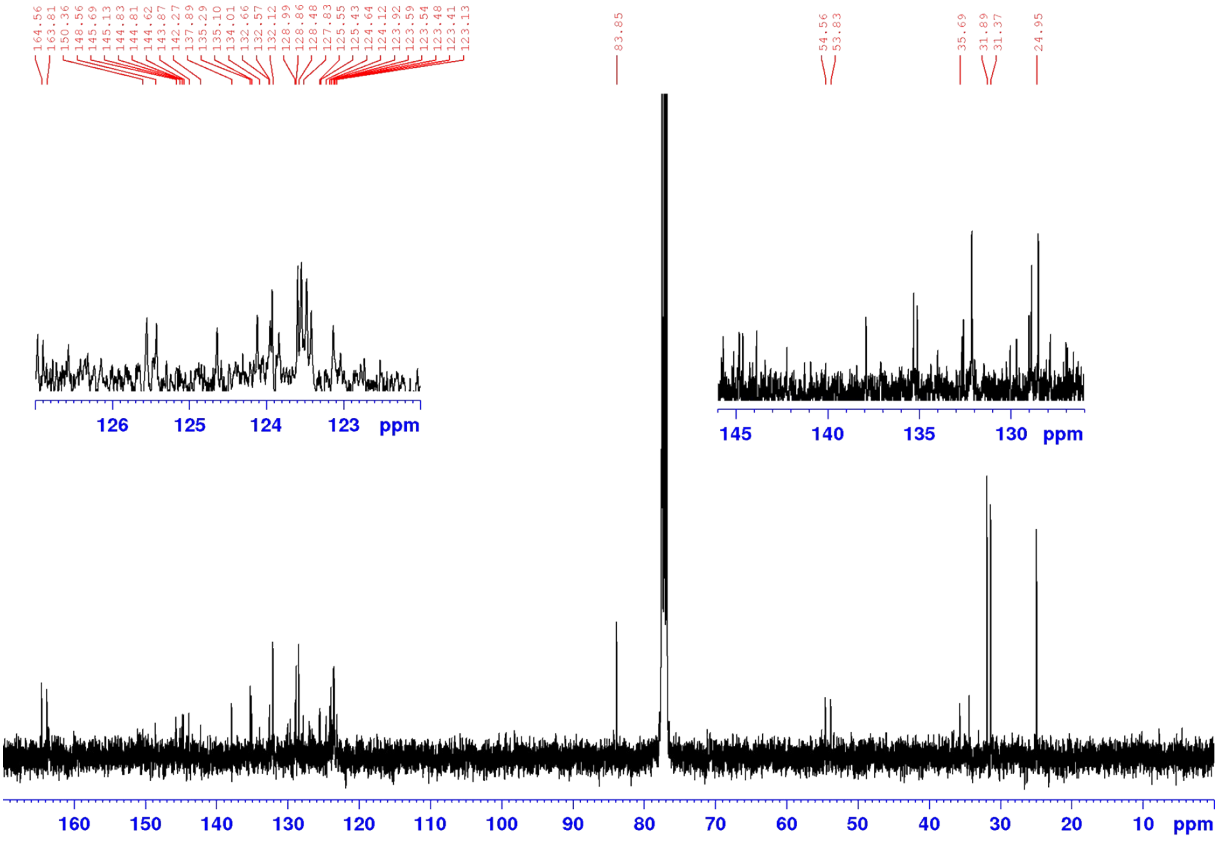

Fig. S6 ^{13}C-NMR: BPin-TTC-PDI ($CDCl_3$, 100.6 MHZ).

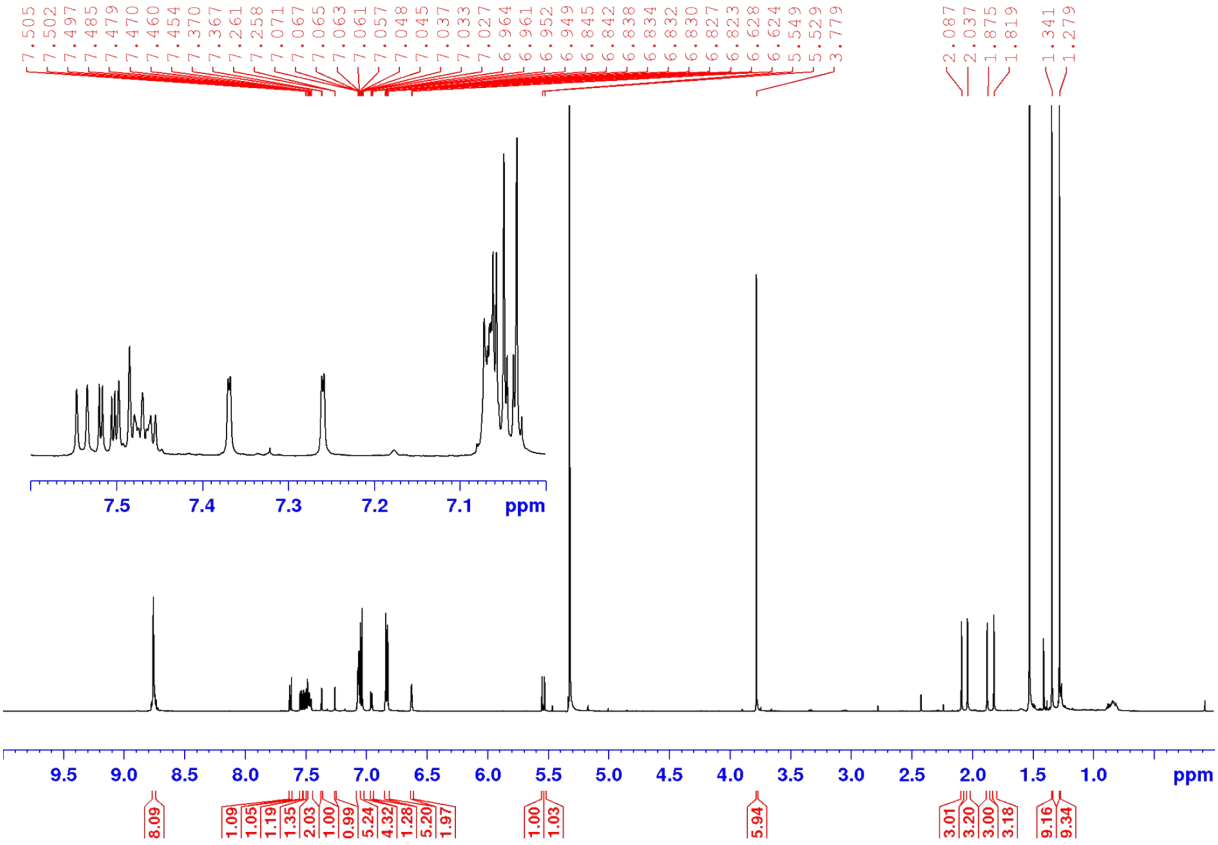

Fig. S7 ^{1}H-NMR: Me23 (CD_2Cl_2, 600.1 MHz).

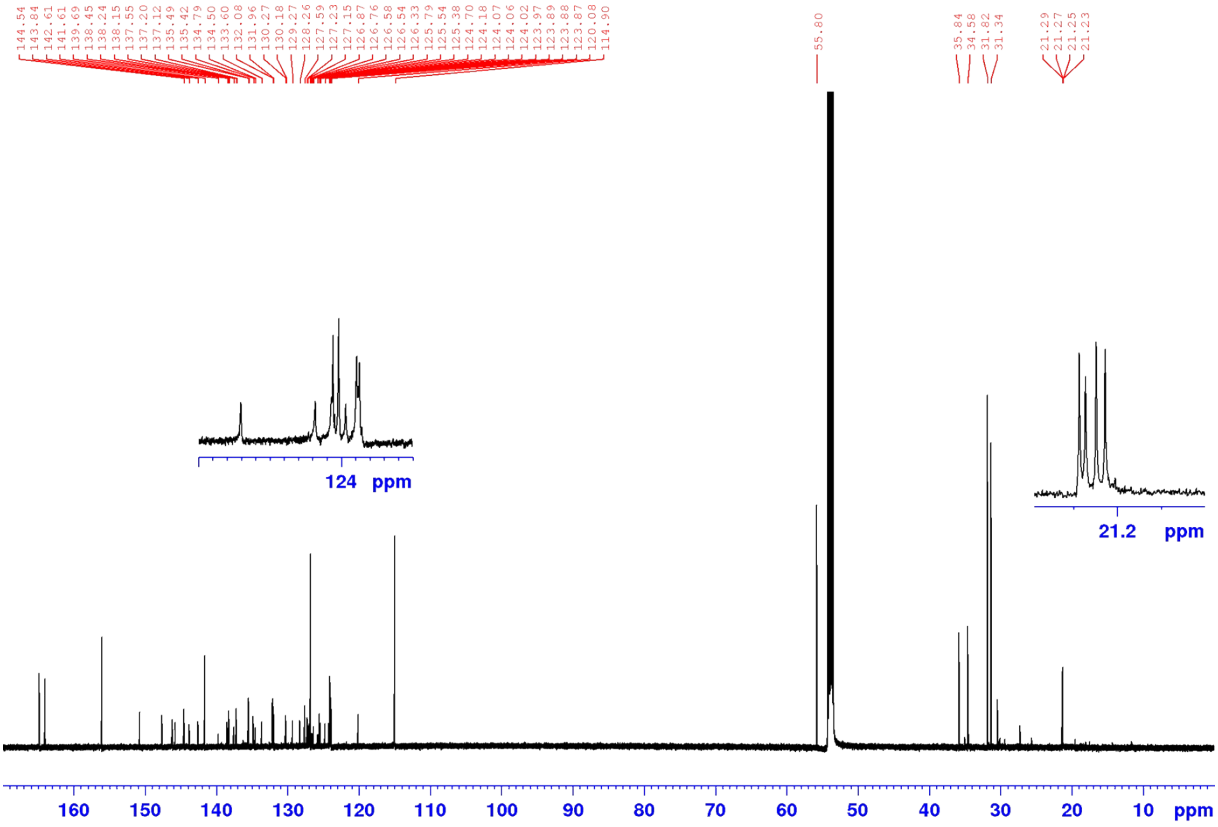

Fig. S8 ^{13}C-NMR: Me23 (CD_2Cl_2, 150.9 MHz).

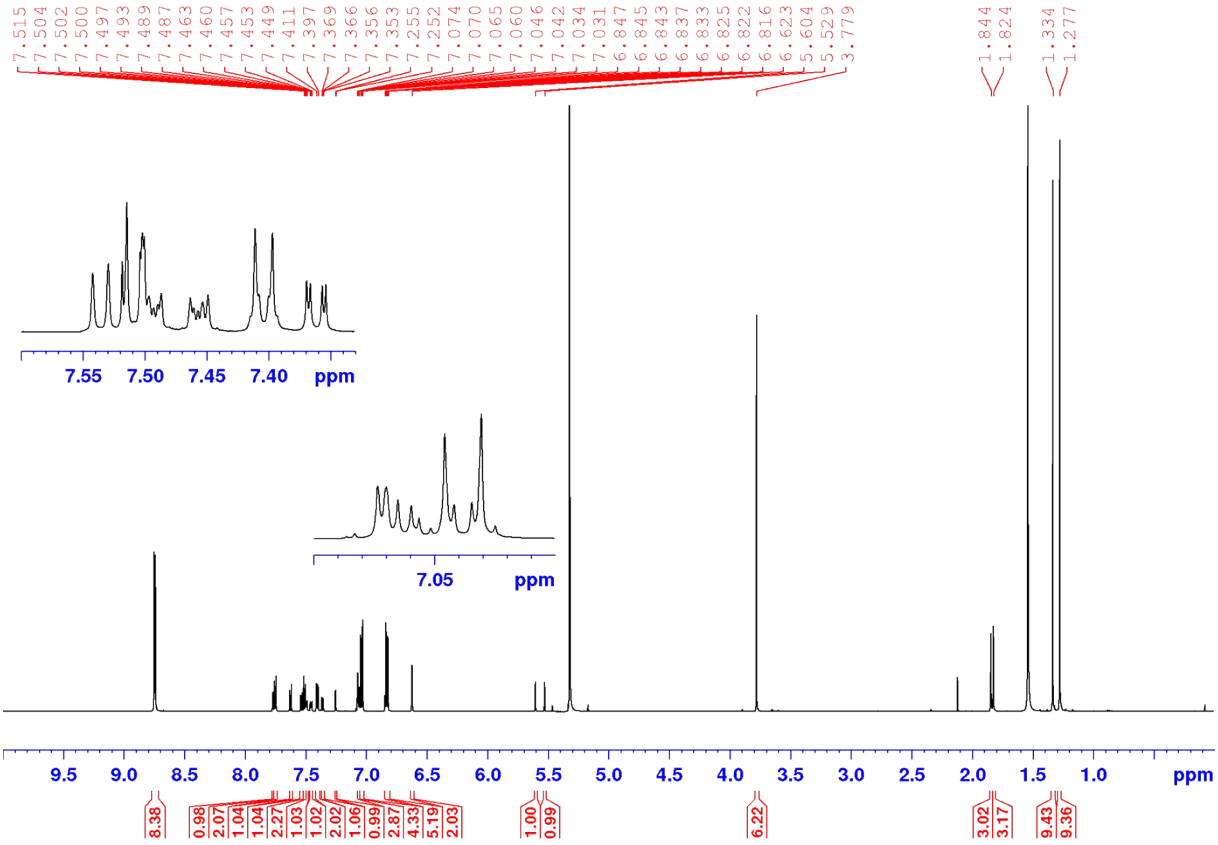

Fig. S9 ^{1}H-NMR: Me2 (CD_2Cl_2, 600.1 MHz).

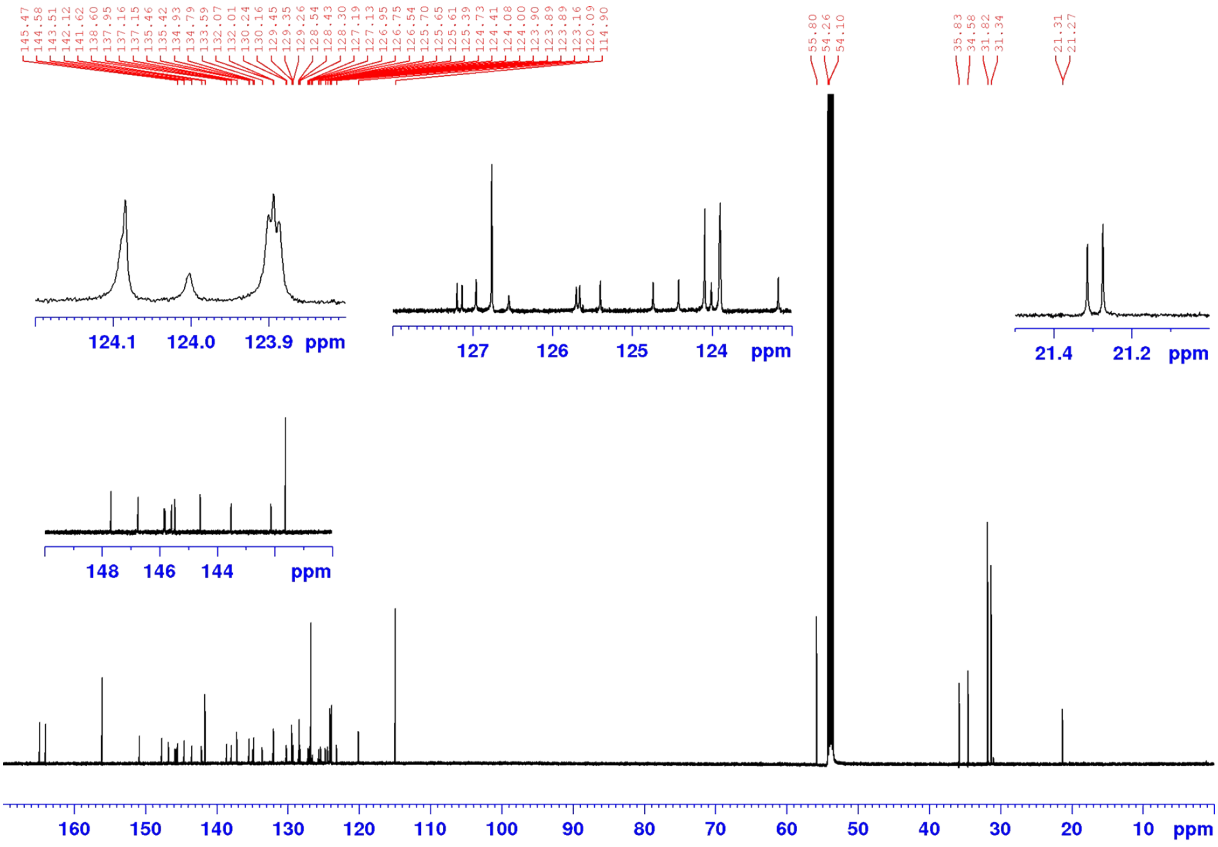

Fig. S10 ^{13}C-NMR: Me2 (CD_2Cl_2, 150.9 MHz).

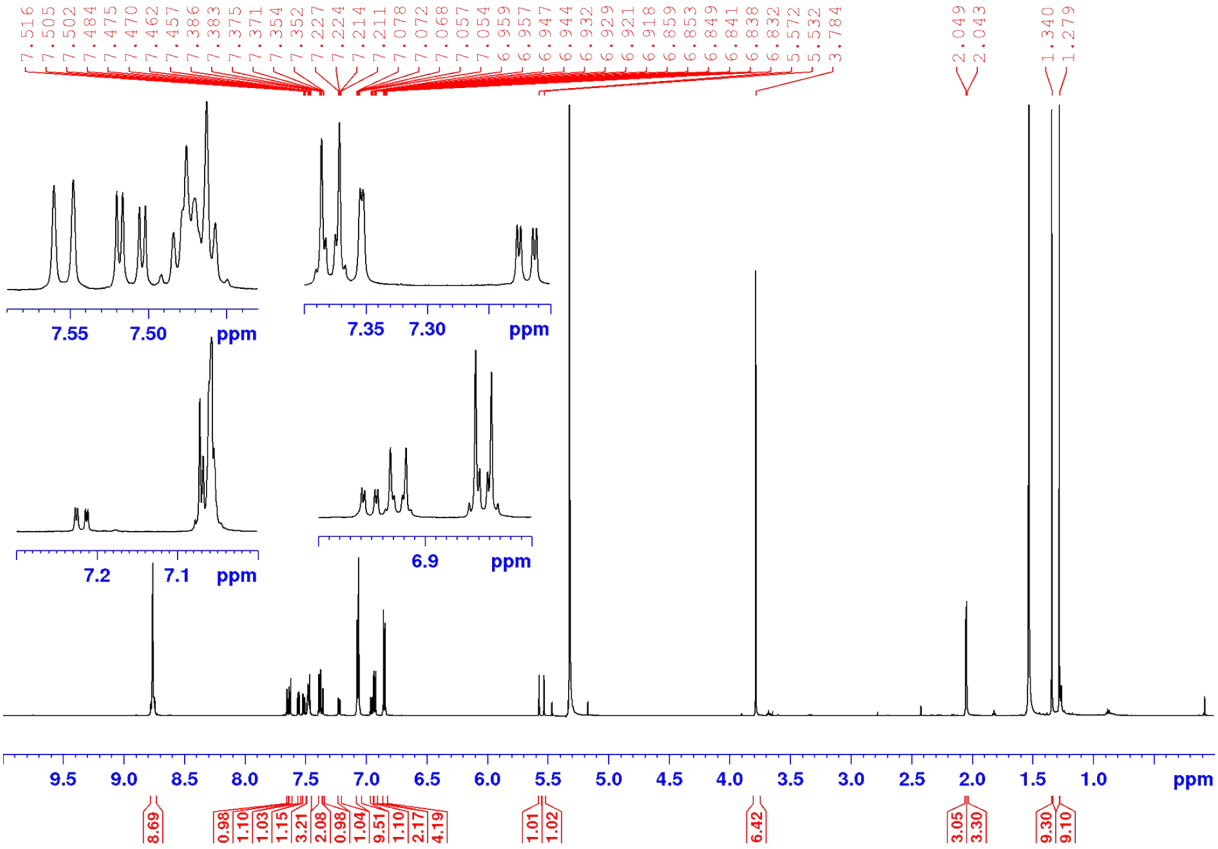

Fig. S11 ^{1}H-NMR: Me3 (CD_2Cl_2, 600.1 MHz).

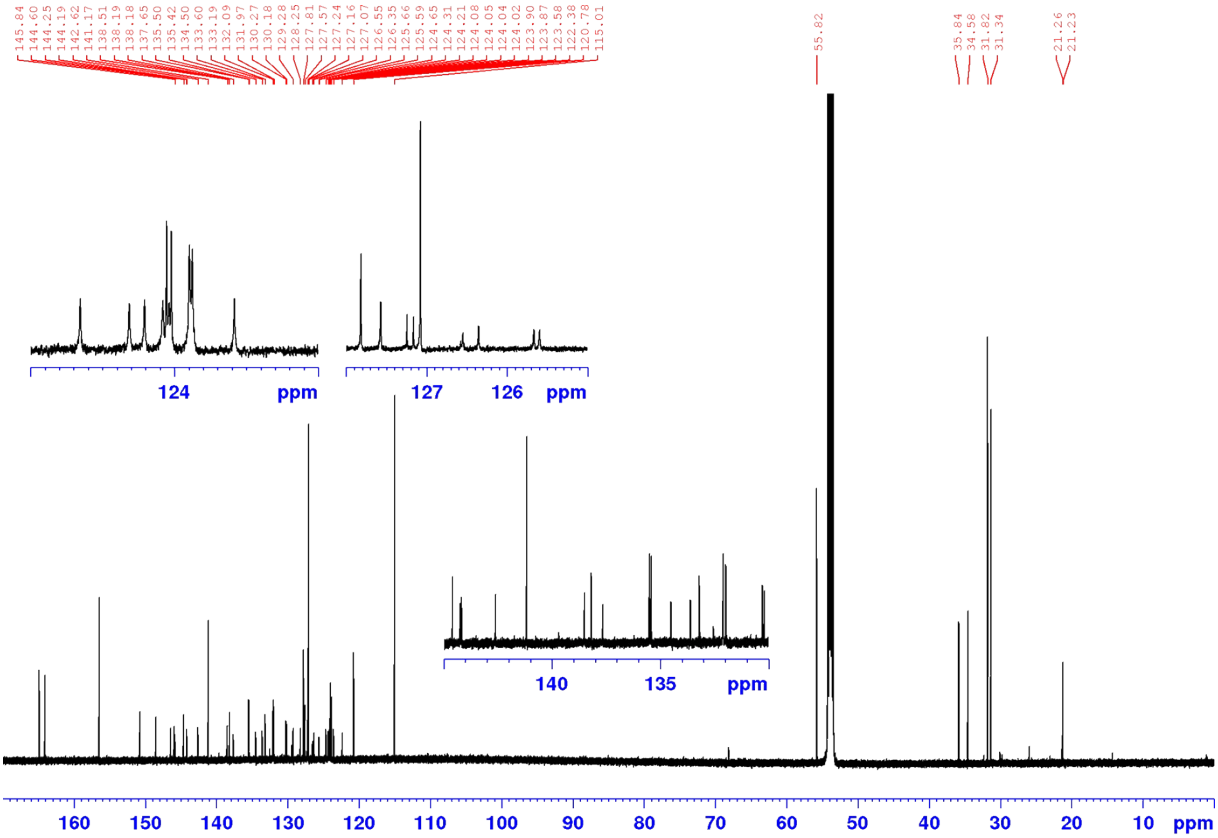

Fig. S12 ^{13}C-NMR: Me3 (CD_2Cl_2, 150.9 MHz).

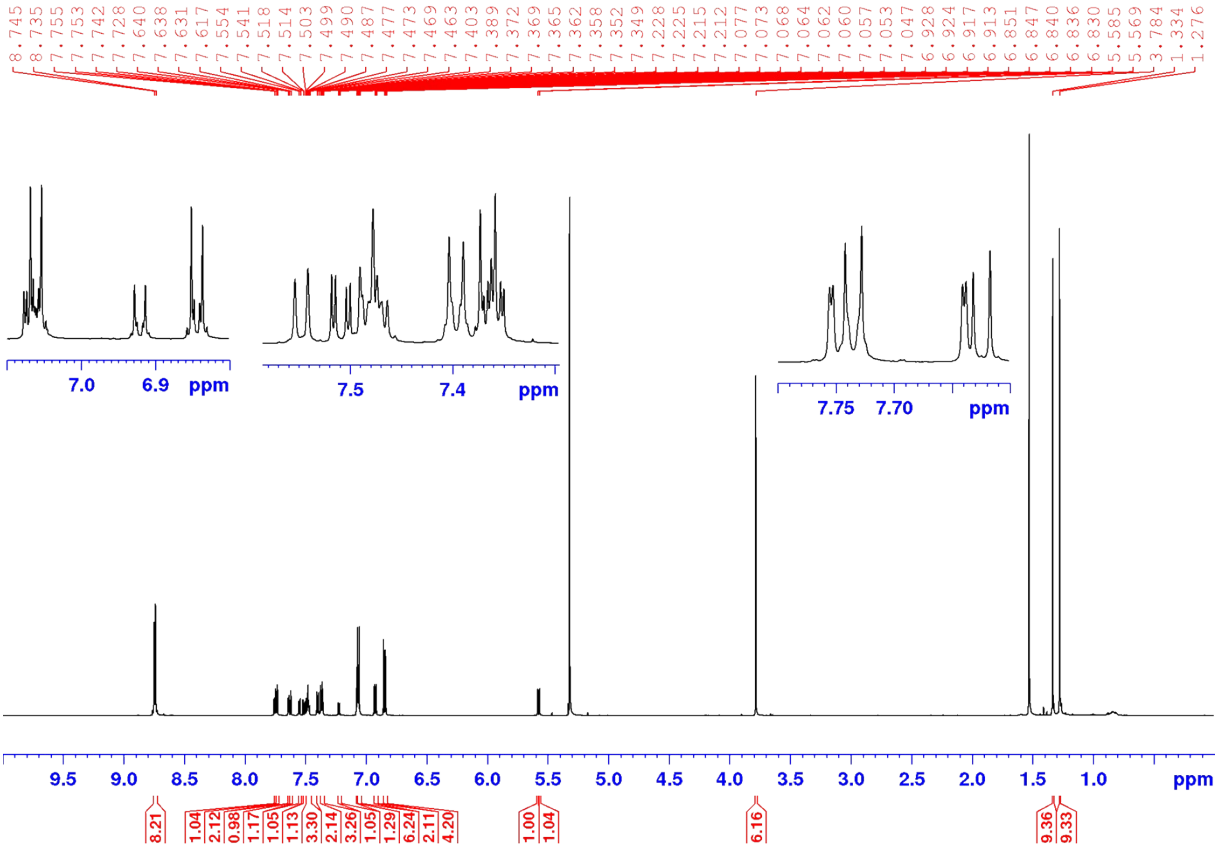

Fig. S13 ^{1}H-NMR: Me0 (CD_2Cl_2, 600.1 MHz).

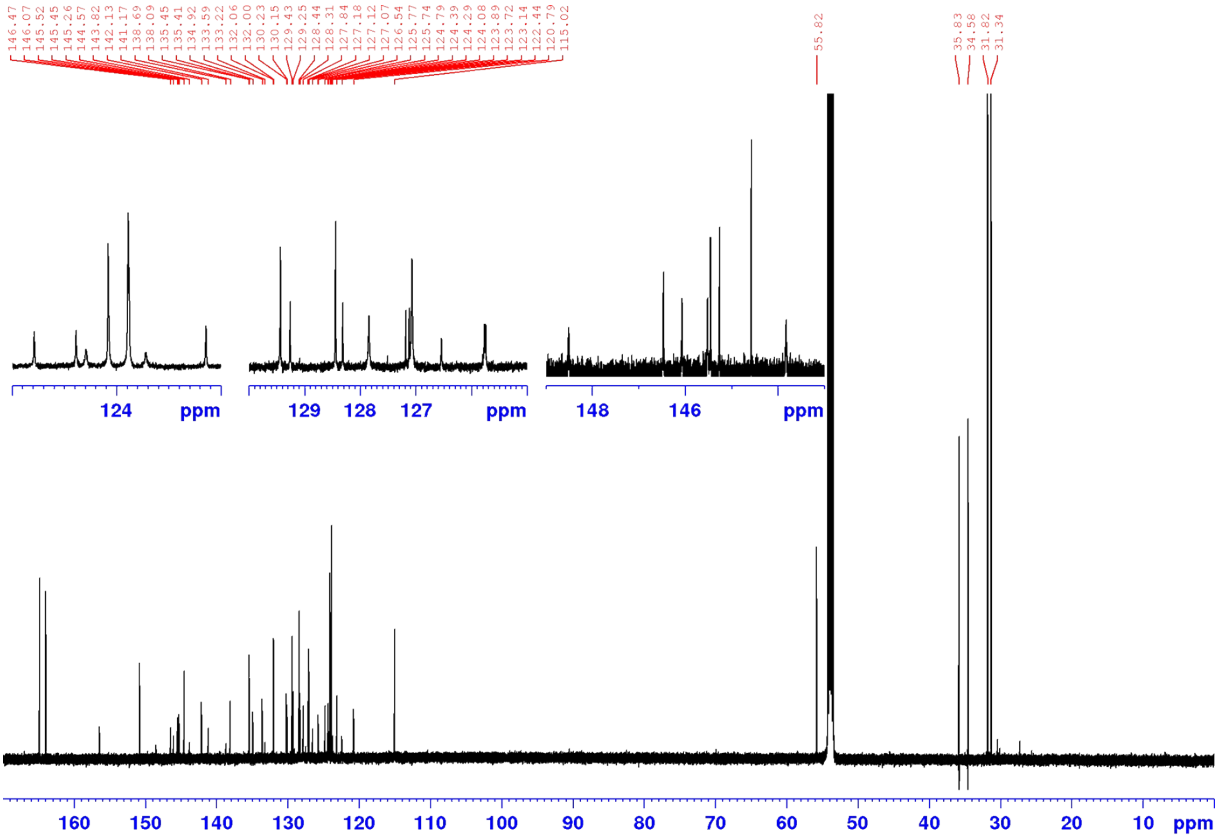

Fig. S14 ^{13}C-NMR: Me0 (CD_2Cl_2, 150.9 MHz MHz).

2. Steady State Absorption and Emission Spectroscopy

2.1. Steady-State Absorption Spectroscopy (UV/Vis)

Absorption spectra were recorded on a JASCO V-670 UV/Vis/NIR spectrometer using spectroscopic grade solvents from Sigma Aldrich and Acros Organics in 10 × 10 mm quartz-cuvettes from Starna. A cuvette with pure solvent was used as reference. In the examined concentration range of 10^{-7} – 10^{-5} M no concentration dependent effects were observed.

2.2. Steady-State Emission Spectroscopy

Emission spectroscopy was measured at r.t. in 10 × 10 mm quartz-cuvettes from Starna using an Edinburgh Instruments FLS980 fluorescence lifetime spectrometer equipped with a 450 W Xenon lamp and a single photon counting photomultiplier R928P. All solvents were of spectroscopic grade (Sigma Aldrich, Acros Organics). The optical density of all samples was below 0.05 for the maximum absorption band of the PDI moiety.

Fluorescence quantum yields were determined using a calibrated integrating sphere and corrected for self-absorption.[8]

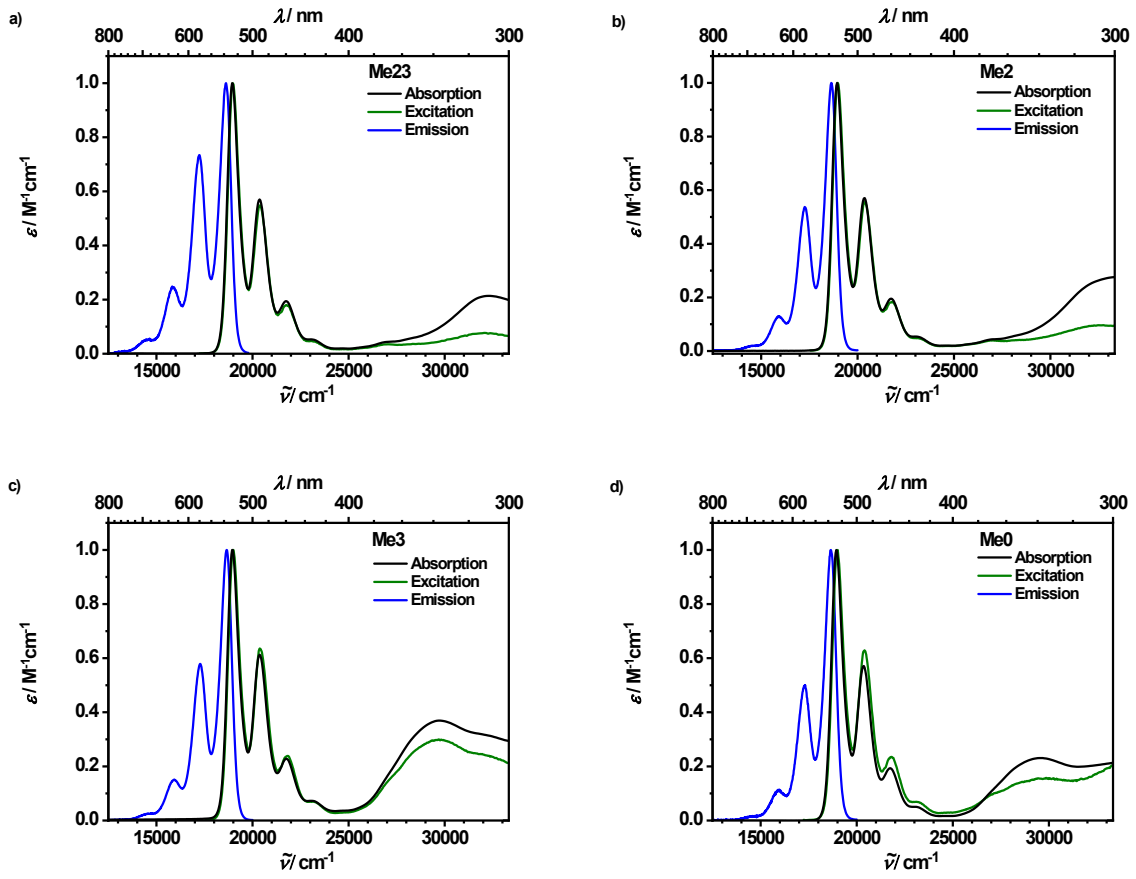

Fig. S15 Absorption- (black), excitation- (green) and emission spectra (blue) of all four triads in toluene at r.t. Emission and excitation spectra were recorded at a concentration of 5 × 10^{-6} mol l^{-1} and the absorption spectra at 1 × 10^{-5} mol l^{-1}.

Tab. S1 Absorption data of all triads in toluene.

	$\tilde{\nu}_{maxPDI}$ / cm^{-1} (λ_{max} / nm)	ε_{max} / $M^{-1}cm^{-1}$	$\tilde{\nu}_{maxTAA}$ / cm^{-1} (λ_{max} / nm)	ε_{max} / $M^{-1}cm^{-1}$
Me23	18900 (528)	79900	32300 (309)	29200
Me2	18900 (528)	84400	-	-
Me3	18900 (528)	83000	29700 (336)	30600
Me0	18900 (528)	84500	29600 (337)	30500

Tab.S2 Emission maxima and fluorescence quantum yields in toluene at 298 K.

	$\tilde{\nu}_{maxPDI}$ / cm^{-1} (λ_{max} / nm)	Φ_{em}
Me23	18600 (537)	0.26
Me2	18600 (537)	0.04
Me3	18600 (537)	0.11
Me0	18600 (537)	0.05

3. Cyclic Voltammetry (CV)

For electrochemical measurements a Gamry Instruments Reference 600 Potentiostat/Galvanostat/ZRA (v. 6.2.2) with a conventional three electrode setup (platinum disc working electrode Ø = 1 mm, Ag/AgCl 'LEAK FREE' reference electrode, platinum wire as counter electrode) was used. The measurements were performed under an argon atmosphere in DCM with 0.2 M tetrabutyl ammonium hexafluorophosphate (TBAHF) as supporting electrolyte at a concentration of a few mM and referenced against the ferrocene/ferrocenium (Fc/Fc^+) redox couple. To check chemical and electrochemical reversibility multiple thin layer experiments were performed.

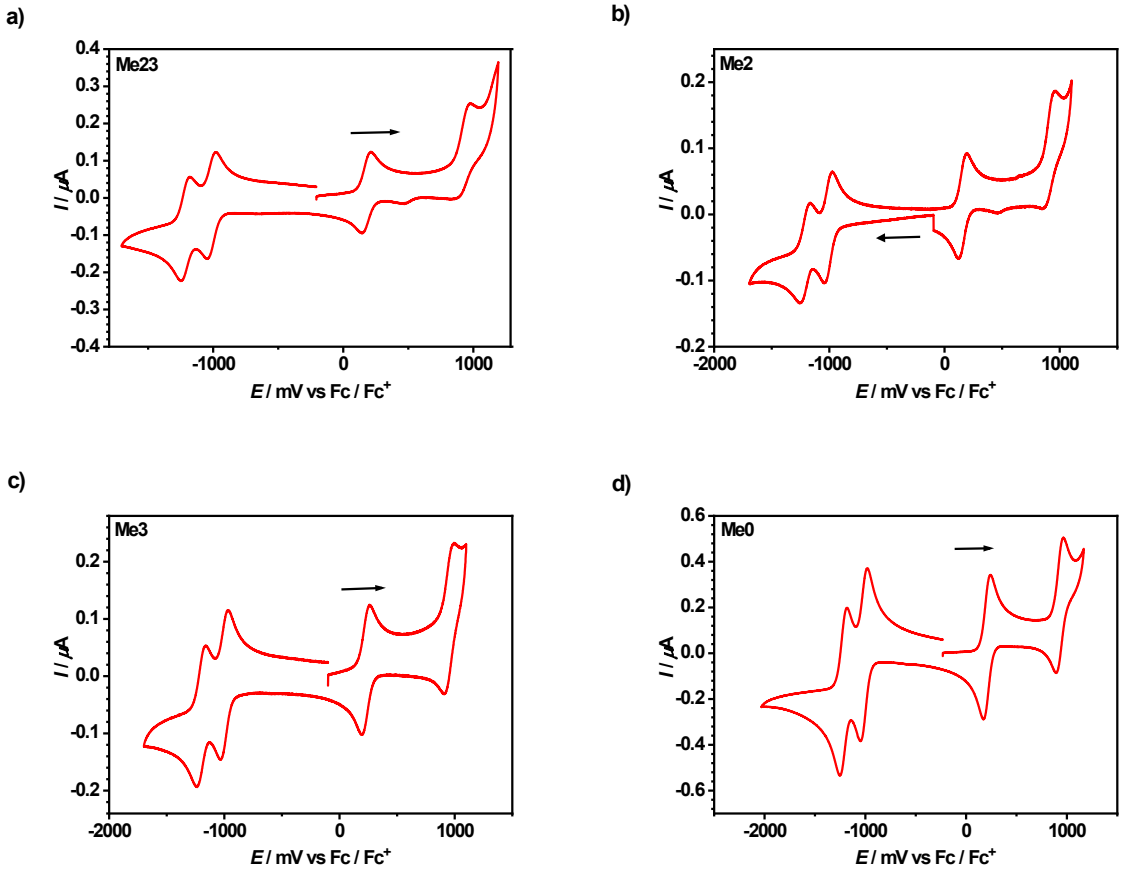

Fig. S16 Cyclic voltammograms of all four triads in DCM containing 0.2 M TBAHF and referenced against Fc/Fc^+.

Tab. S3 Electrochemical data in DCM at r.t. containing 0.2 M TBAHF and referenced against Fc/Fc^+.

	$E_{1/2}$ / mV			
	Ox_1	**Ox_2**	**Red_1**	**Red_2**
Me23	180	929[a]	-1011	-1212
Me2	164	909[a]	-1015	-1224
Me3	230	951[a]	-997	-1200
Me0	210	932[a]	-1012	-1216

[a] chemically irreversible

4. Gibbs-Energies of CS State from the Weller Approach[9] and Reorganisation Energies

$$\Delta G_{1_{CS}}^{0} = \frac{N_A}{1000} Ze\left(E_{Ox}(D/D^+) - E_{red}(A/A^-)\right) -$$

$$\frac{N_A e^2}{1000 \times 4\pi\varepsilon_0}\left[\left(\frac{1}{2r_D} + \frac{1}{2r_A}\right)\left(\frac{1}{\varepsilon_r} + \frac{1}{\varepsilon_s}\right) + \frac{1}{\varepsilon_s d_{DA}}\right]$$

(1)

The energy gap of the final charge separated state and the ground state corresponds to the redox potential difference of the donor and the acceptor (in Volt). Their potentials were determined by cyclic voltammetry and are given in Table S3. Eqn 1 includes a Coulomb term which takes into account that the separated charges are extra stabilised by Coulomb attraction. In this term r_D and r_A are the radii of the donor and acceptor which were calculated from the corresponding Connolly Molecular Surfaces of the subunits optimization with Chem3D Ultra [10] and the centre to centre distance between them (in Meter). The donor-acceptor distances r_{DA} were determined at a B3LYP/6-31G* level of theory using Gaussian09.[11] N_A is Avogadro's constant, e the elementary charge, z the number of transferred charges. ε_0 is the vacuum permittivity, ε_r is the permittivity of the solvent used for cyclic voltammetry and ε_s is that for the solvent used in the photophysical experiment.

Internal reorganisation energies λ_i for CR (CS → S_0) were estimated from DFT calculations at B3LYP/6-31G* level of theory via the NICG (neutral in cation geometry) method [12, 13] and outer reorganization energies λ_o were calculated based on the Born model. [14, 15]

State Energy Diagram

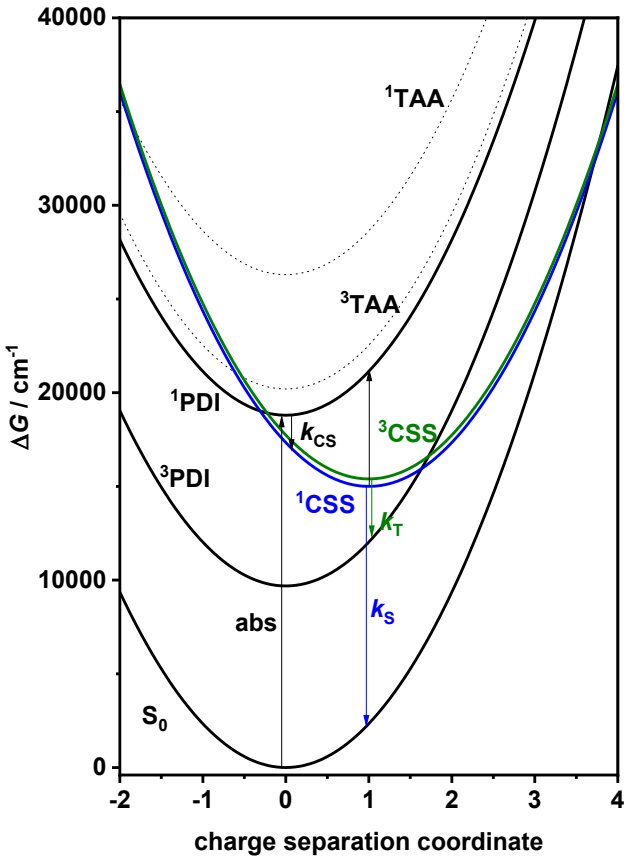

Fig.17 State energy diagram of all states involved in charge separation and recombination with their respective reorganisation energy parabolas. Charge transfer processes are indicated as vertical arrows starting at the equilibrium position of the pertinent initial states. The reorganisation energy was estimated to be 2339 cm^{-1} by DFT calculations. Energies were taken from Table 1 and ref. 15

5. Transient Absorption Spectroscopy

5.1. fs-Transient Absorption Spectroscopy

The Transient absorption setup (TAS) consists of a one-box femtosecond laser system "Solstice" from Newport Spectra Physics, a "HELIOS" transient absorption spectrometer (TASp) from Ultrafast Systems, a home-built NOPA, and a "TOPAS-C" from LightConversion. The fundamental wavelength from the Solstice is 800 nm with a repetition rate of 1 kHz and a pulse length of 100 fs. The HELIOS spectrometer has two channels, one for measurement and one for the reference. Furthermore, it is equipped with a fibre-coupled linear CMOS sensors with a sensitivity from 315 nm to 925 nm and an intrinsic spectral resolution of 1.5 nm. The white light continuum (WLC) is created by an oscillating 3 mm thick CaF_2 crystal which was

pumped by the TOPAS-C output at 1000 nm to obtain a gapless WLC from 340 nm to 915 nm. The probe wavelength range was chopped with a 400 nm long pass filter and a 900 nm short pass filter to reach the evaluated region from 420 nm – 870 nm. The pump beam from the TOPAS-C for the WLC is guided over a linear stage which provides a time delay up to 7 ns. The step size for the first 4 ps is 20 fs and afterwards the steps increase exponentially up to 200 fs. The measurements were carried out under magic angle conditions. The angle between the polarization directions between pump and probe was 54.7° and the angle in space between both beams was 10°. The pump beam for the sample was produced by a home-built NOPA at 528 nm and the pulse lengths were shorter than 40 fs in a Gaussian fit and the pulse shape was close to the bandwidth limitation. The instrument response function derived from the coherent artefact was ca. 100 fs. All samples were dissolved in toluene from Merck and measured in a cuvette with an optical path length of 0.2 mm, a window thickness of 0.1 mm and pumped with 30 nJ.

GLOTARAN (v. 1.2) was used to analyse the recorded time resolved spectra by a global deconvolution using a sequential model to yield evolution associated difference spectra (EADS).[16] By fitting a third order polynomial to the cross-phase modulation signal of the pure solvent the white light dispersion (chirp) was corrected.

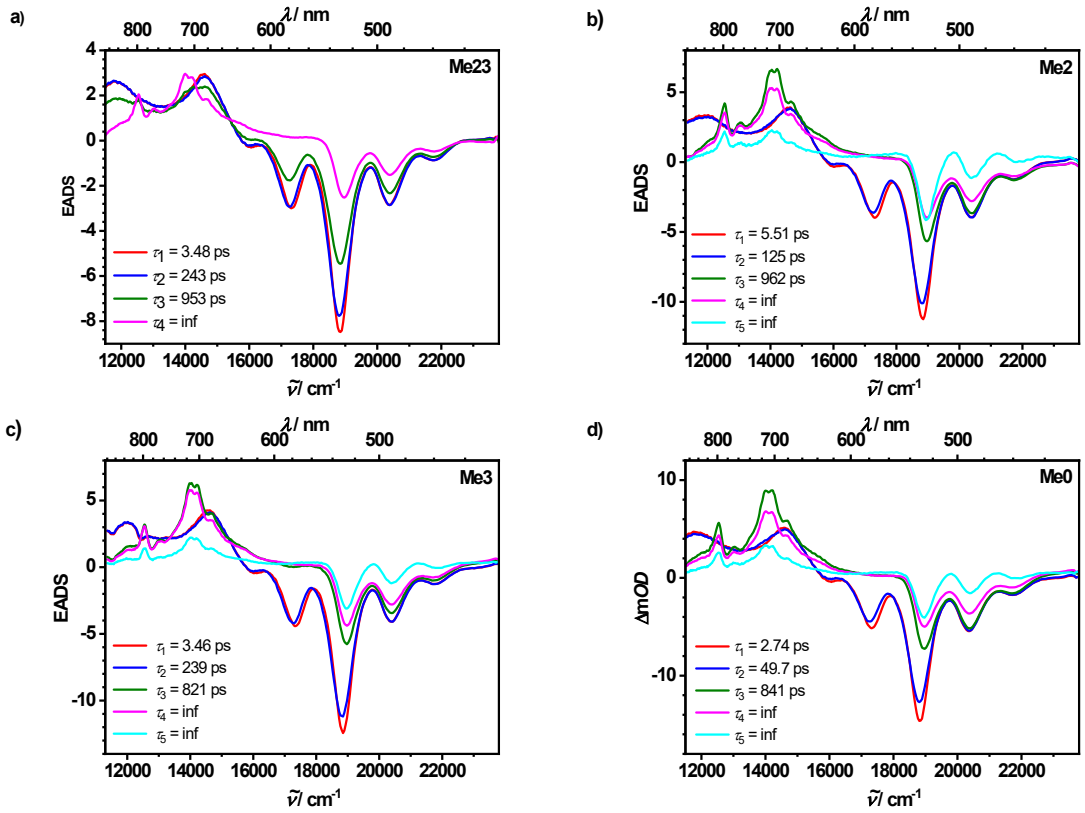

Fig. S18 *Evolution associated difference spectra* (EADS) in toluene at 298 K after pumping at 18900 cm^{-1} (528 nm) and probing with continuous withe light between 11500 cm^{-1} (870 nm) and 23800 cm^{-1} (420 nm).

5.2. Target Fits

For processing a target fit of the transient map we can safely assume that at 490 nm the EADS of excited PDI and the PDI radical anion only show GSB and no superimposed ESA or SA. However, this is not true for the triplet PDI as this shows a strong ESA in this spectra region. Therefore, species associated difference spectra (SADS) of the singlet PDI and the CS state should possess the same (but unknown) extinction coefficient at 490 nm. Therefore, in a global target fit, we adjusted the efficiencies of depopulation channels of all pertinent states in a way, that this criterion concerning the extinction coefficient was met. In doing so, the rate constant for depopulation of a specific state changed during the global fit in comparison to the evolution associated difference spectra where a sequential model was assumed, and all efficiencies are unity. The rate constants for the charge separation channel are then given as the quotient of the efficiency of the charge separation channel and the lifetime of the excited PDI state.

Me0

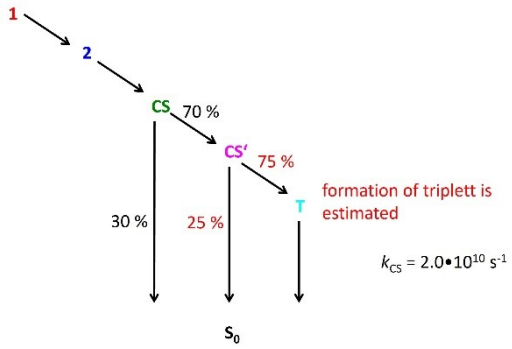
1
2
CS
70 %
CS'
75 %
T
30 %
25 %
S0
formation of triplett is estimated
kCS = 2.0•10^10 s^-1

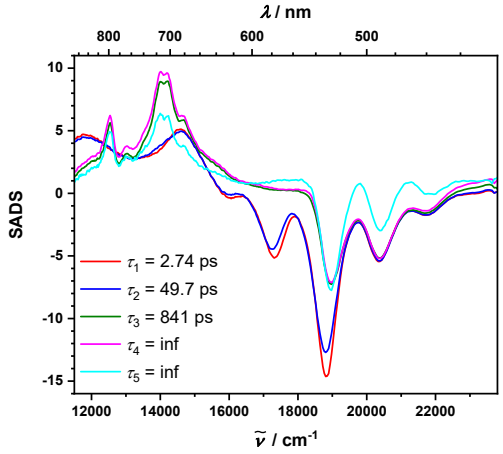
λ / nm
800
700
600
500
SADS
τ1 = 2.74 ps
τ2 = 49.7 ps
τ3 = 841 ps
τ4 = inf
τ5 = inf
ν̃ / cm-1

Me2

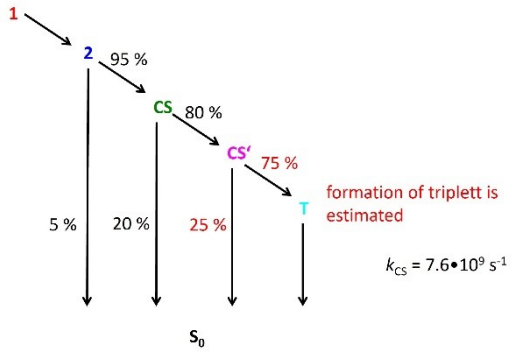
1
2
95 %
CS
80 %
CS'
75 %
T
5 %
20 %
25 %
S0
formation of triplett is estimated
kCS = 7.6•10^9 s^-1

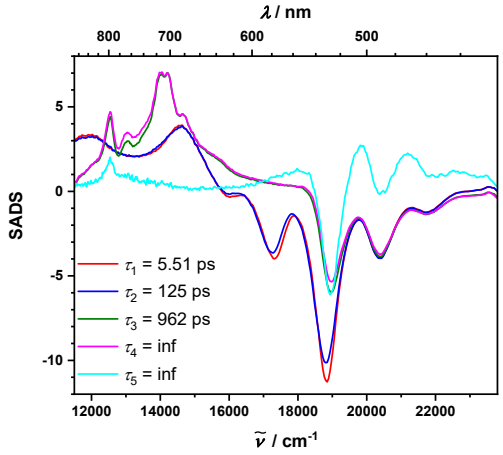
λ / nm
800
700
600
500
SADS
τ1 = 5.51 ps
τ2 = 125 ps
τ3 = 962 ps
τ4 = inf
τ5 = inf
ν̃ / cm-1

Me3

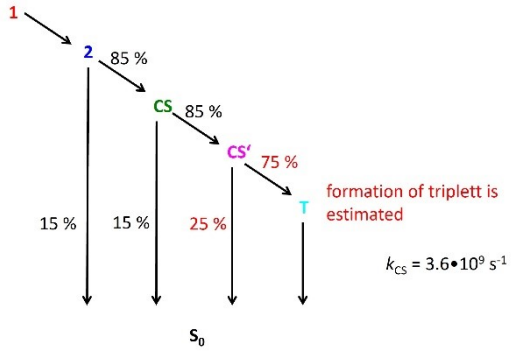
1
2
85 %
CS
85 %
CS'
75 %
T
15 %
15 %
25 %
S0
formation of triplett is estimated
kCS = 3.6•10^9 s^-1

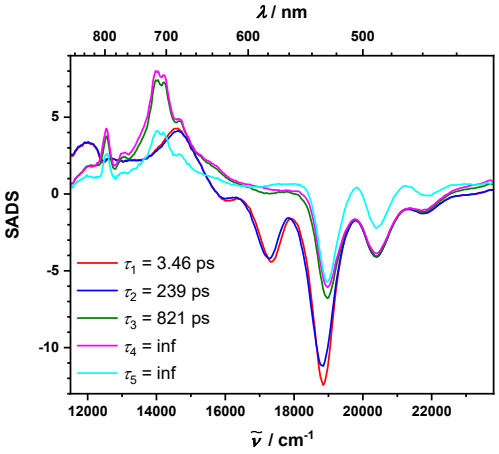
λ / nm
800
700
600
500
SADS
τ1 = 3.46 ps
τ2 = 239 ps
τ3 = 821 ps
τ4 = inf
τ5 = inf
ν̃ / cm-1

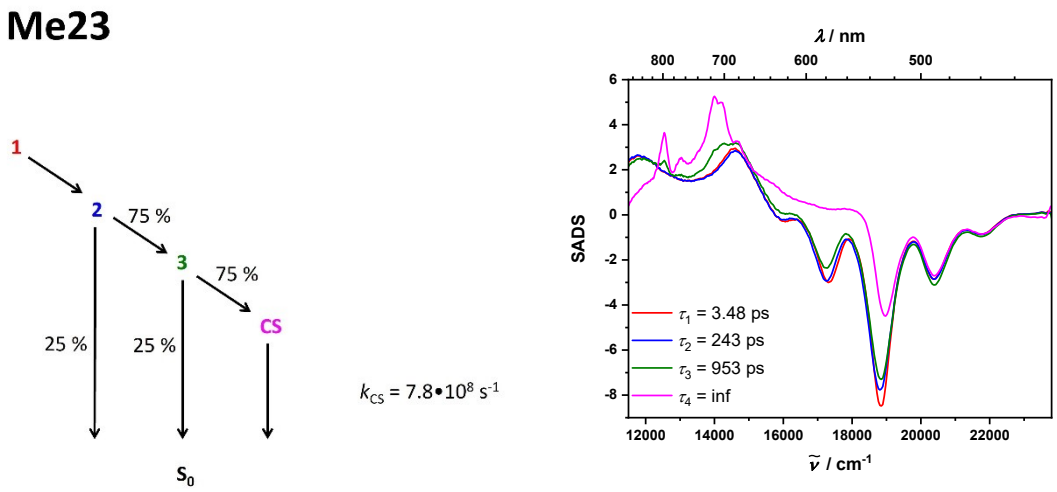

Fig S19 Target fits of the transient maps under the assumption that all SADS spectra match at ca. 490 nm.

5.3. ns-Transient Absorption Spectroscopy

An Edinburgh LP 920 laser flash spectrometer using an EKSPLA NT340 Nd:YAG laser with integrated optical parametric oscillator was used to perform the ns-transient absorption spectroscopy measurements. The white light was generated by a 450 W Xe arc flash lamp whereby the white light and the pump light beams were perpendicular to each other. The solvent was of spectroscopic grade from Sigma Aldrich and degassed by 7 freeze pump thaw cycles. Sample preparation was carried out in a nitrogen filled glovebox in 10 x 10 mm quartz-cuvettes equipped with a *Young's* valve. No bimolecular processes were observed in a concentration range of 10^{-6} to 10^{-5} M. All samples were excited with ca. 5 ns laser pulses (ca. 1.2 mJ pulse energy) with a 10 Hz repetition rate. They were excited at the maximum ground state absorption of the respective PDI moiety at 18900 cm^{-1} (528 nm). Measuring temporal decay profiles in 10 nm steps between 25000 cm^{-1} (400 nm) and 12500 cm^{-1} (800 nm) gave the transient maps. The decay profiles were also corrected by fluorescence and the decay curves were fitted by the spectrometer L900 software.

The magnetic field dependent measurements were performed using a GMW Associates C-frame electromagnet 5403 (pole diameter = 76 mm, pole face = 38 mm, axial hole in poles 6.35 mm, pole gap = 13 mm) implemented in the aforementioned laser set-up. To control the magnetic field strength a Hall-sensor (Single-Axis Magnetic Field Transductor YM12-2-5-5T, SENIS GmBH) was used. The error of the magnetic fields was determined to be <0.02 mT between 0 – 400 mT and <1 mT between 400 – 1800 mT by placing the Hall-sensor at the pole face and correcting them by the previously recorded calibration curve. The stability of all samples was checked by repeatedly testing selected magnetic fields as well as comparing

steady-state absorption spectra that were recorded at the beginning and the end of all measurements.

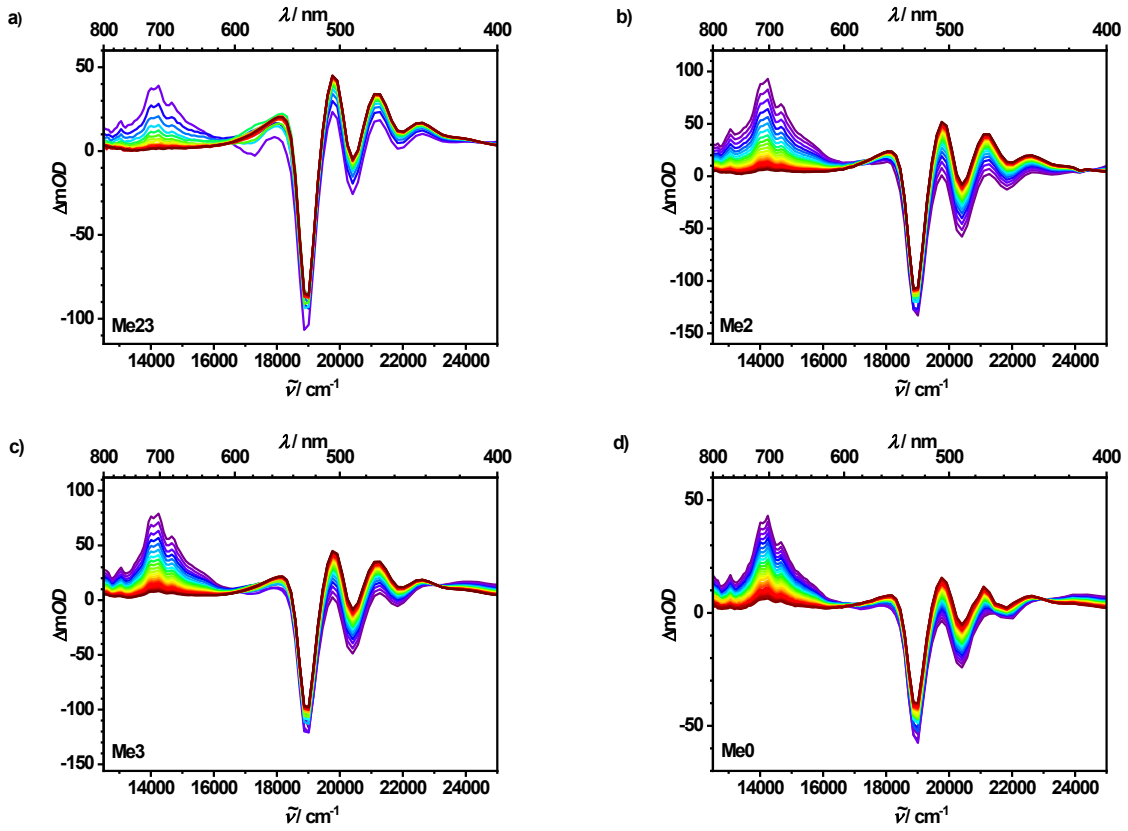

Fig. S20 ns-transient maps in toluene at 298 K after excitation at 18900 cm^{-1} (528 nm) and probing with continuous withe light between 12500 cm^{-1} (800 nm) and 25000 cm^{-1} (400 nm). The displayed spectra are at 7 ns steps with early times shown in purple and later times in red.

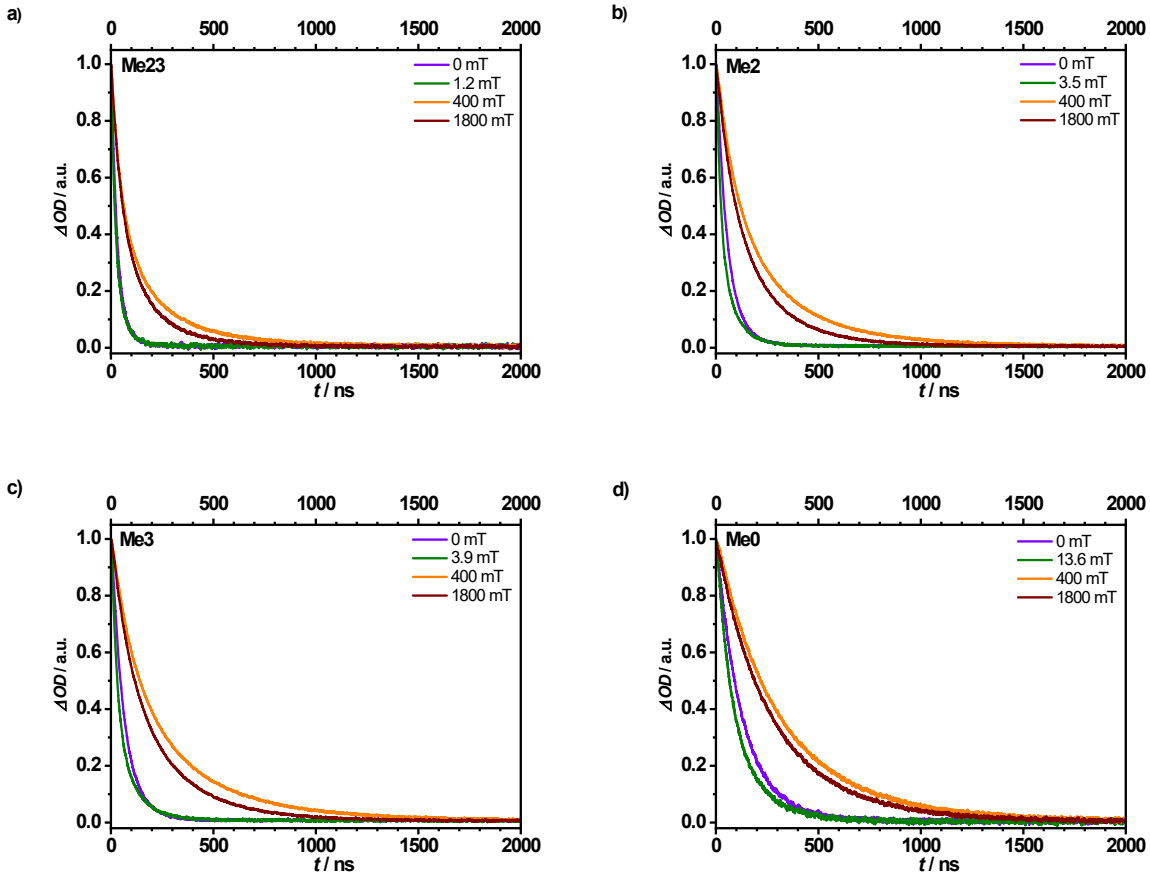

Fig. S21 Transient absorption decay profiles at selected magnetic fields for all triads in toluene at 298 K after pumping at 18900 cm^{-1} (528 nm) and probing at 14100 cm^{-1} (710 nm).

Tab. S5: Lifetimes at selected magnetic fields (see Fig. S21) in toluene at 298 K.

	0 mT τ_1 / ns (a_1) τ_2 / ns (a_2)	**2*J*** τ_1 / ns (a_1) τ_2 / ns (a_2)	**1800 mT** τ_1 / ns (a_1) τ_2 / ns (a_2)
Me23	29 (0.97) 117 (0.03)	21 (0.86) 66 (0.14)	46 (0.58) 163 (0.42)
Me2	46 (0.88) 95 (0.12)	20 (0.71) 80 (0.29)	66 (0.39) 199 (0.61)
Me3	53 (0.84) 104 (0.16)	25 (0.69) 97 (0.31)	80 (0.39) 238 (0.61)
Me0	129 -	54 (0.53) 145 (0.47)	99 (0.13) 290 (0.87)

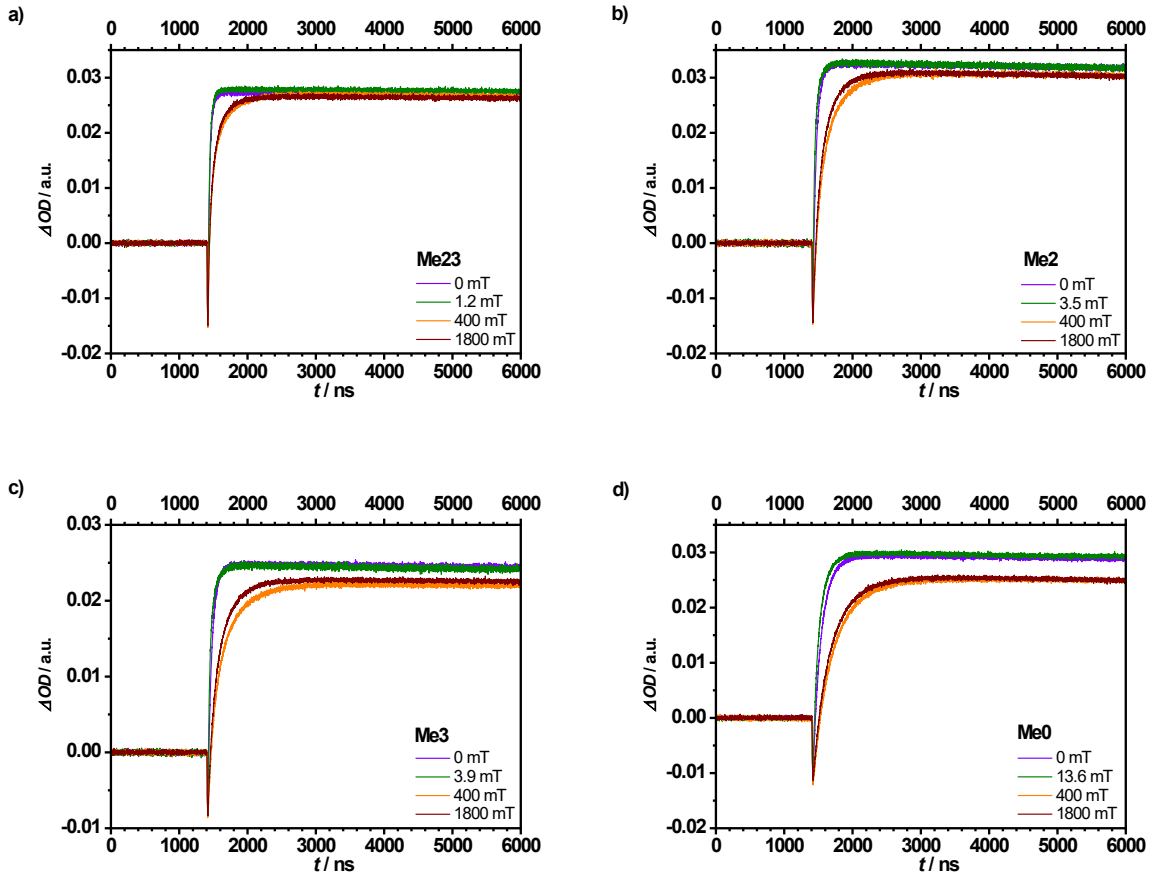

Fig. S22 Transient absorption triplet rise at selected magnetic fields for all triads in toluene at 298 K after pumping at 18900 cm^{-1} (528 nm) and probing at 21300 cm^{-1} (470 nm).

6. Parameter Fitting

The parameter values presented in Table 2 were obtained by successive optimization, whereby the position of the maxima and the widths of the k(B) spectra represented good starting points for $2J$ and k_{STD}, respectively. At the beginning, the parameter T_{long} was set to infinity. Regarding the values of k_S and k_T, we note that the former has a major effect on the ratio between the low-field and high-field values of $k(B)$. The J values are taken to be positive, meaning that the triplet state is below that of the singlet state, in agreement with recent CIDNP measurements[17] and with magnetic field dependent pump-push measurements in comparison with elaborate quantum dynamical calculations of similar triads.[18]

For all compounds, the high field values of $k(B)$ range by more than a factor of 2 below the zero-field values (**Me0**: 2.26, **Me2**: 2.79, **Me3**: 2.84, **Me23**: 2.49) which is only possible if k_S is much smaller than k_T. A limiting value of 3 would be expected for $k_T >> k_S$, however only if k_T were much slower than the S/T conversion process. In a first approach, k_S was set to zero and k_T was chosen to yield the correct zero field kinetics.

Finally, the first order values of k_S are found by adjusting the ratio between zero-field and high-field recombination rates. After fixing the parameters J, k_{STD}, k_S, and k_T to first order, they were successively improved by seeking the minimum deviation from the experimental result through individual variation of the parameters. Examples of the kind of error dependence caused by such variations are shown in Fig. S24 and S25 for **Me0.**

It has been noted in the main text, that the parameters k_S and T_{long} have a completely identical effect on the simulated kinetics. Thus, only combinations of them are uniquely defined by the fits. The functional relationship defined by such combinations is shown in Fig. S23. As k_S increases the curves approach a singularity beyond which no meaningful combination of k_S and T_{long} can be found. The range between zero and the singularity point is taken as the error range of k_S in each case.

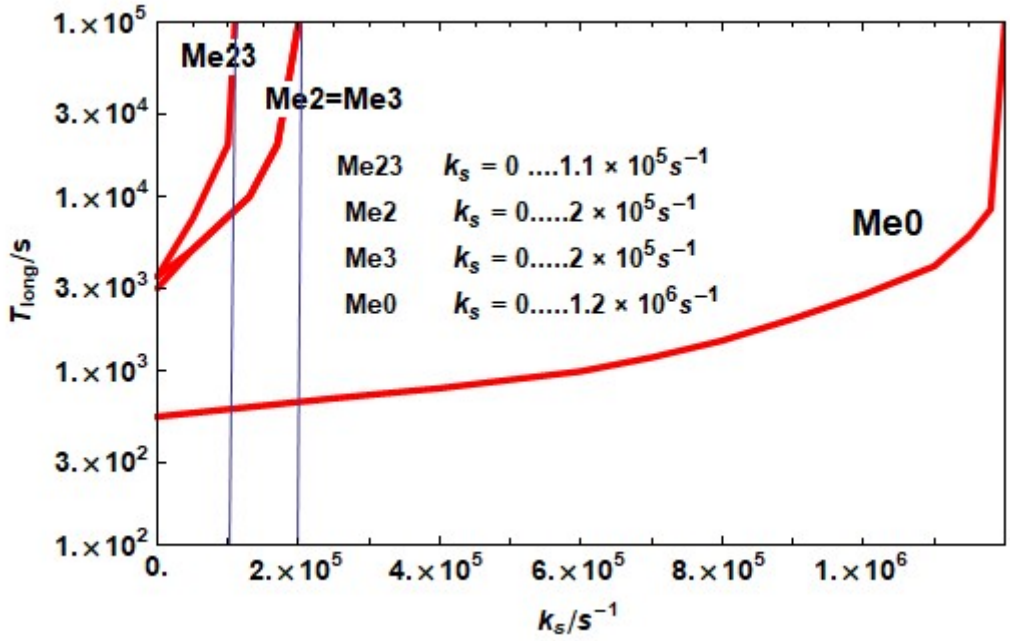

Fig. S23 T_{long} vs k_S as connected by the condition to produce equivalent simulations of $k(B)$.

To some degree, the effects of variations of different parameters may compensate each other also in other cases than k_S and T_{long}. This is particularly true for the parameters J and k_T in the case of **Me23** (cf. Table 2).

7. Error Limits

To standardise the errors related to a certain set of fit parameters, we considered deviations of the calculated $k(B)$ curve from a standard curve for a set of sampling fields, e.g (in case of **Me0**) . 0.01, 0.1, 0.9, 3.1, 5.8, 7.4, 11.5, 13.6, 17.7, 28, 36, 110, 950 mT. As the reference curve we chose the best fit result (cf. Fig. S 24)

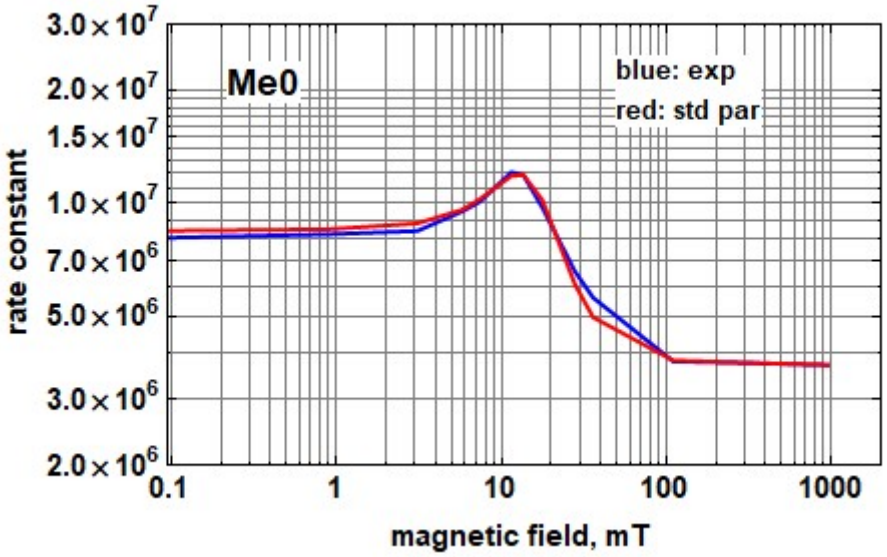

Fig. S24 Experimental and best fit curve used in error estimation in case of **Me0**.

The error values plotted in the following diagrams for the cases of **Me0** represent the rms-value of the deviations between the lg($k(B)$) values of the current fit and standard fit. An error value of 0.05 corresponds to an average factor of 1.12 or 0.88, respectively, between current fit and standard fit.

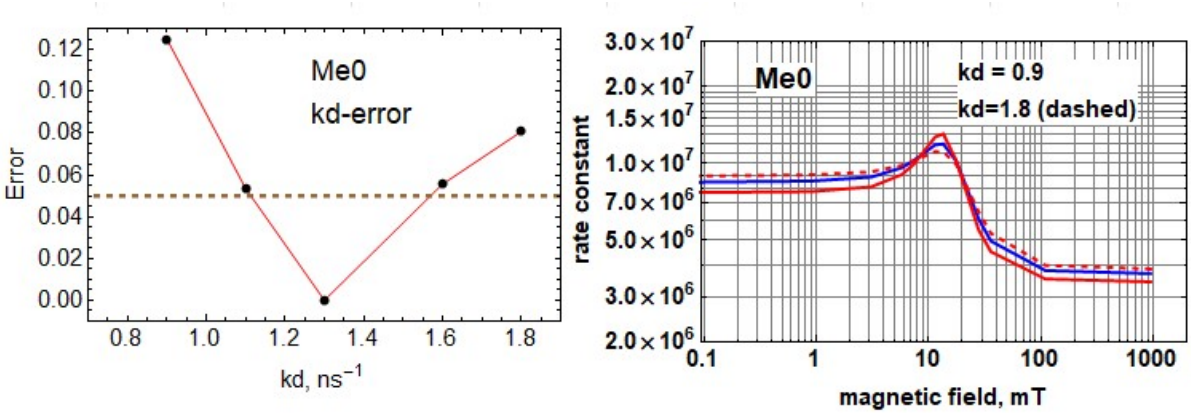

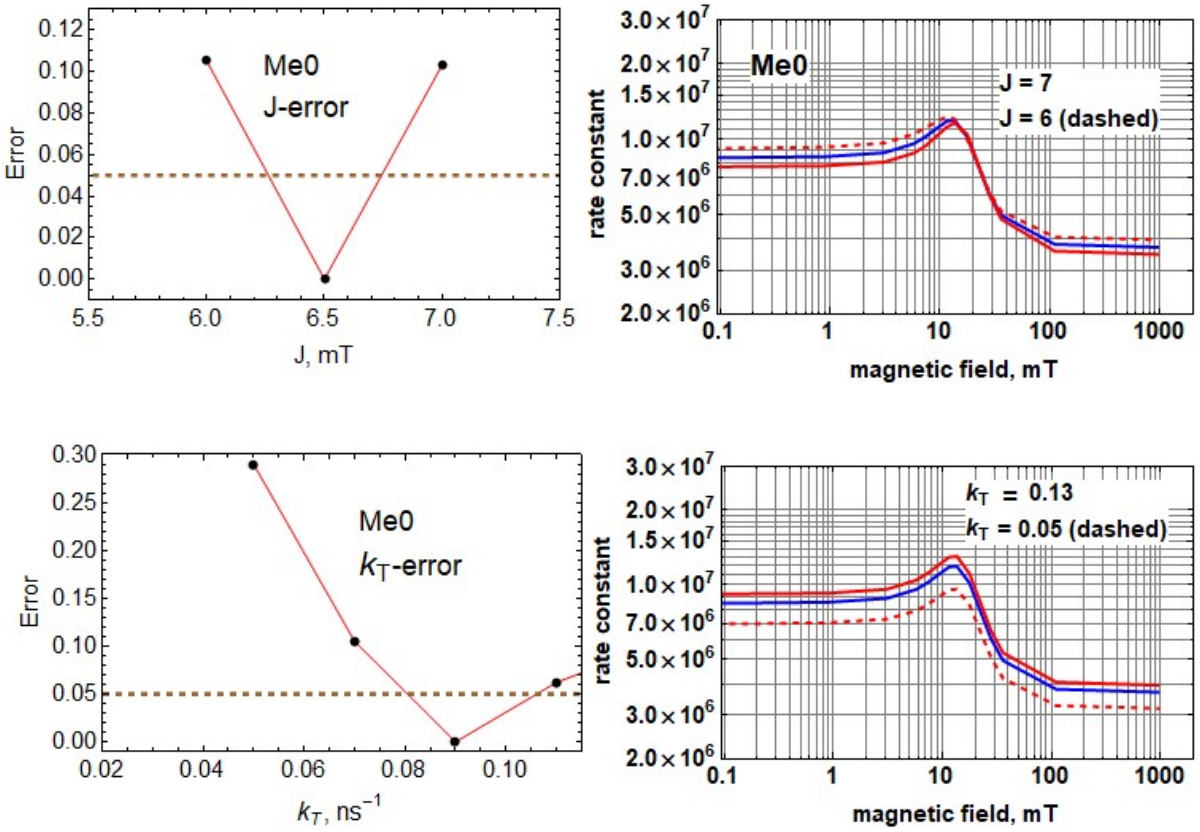

Fig. S25 Left: error estimations for parameters $k_{STD,}$ *J, and* k_T for **Me0**. Right: Standard reference curve $k(B)$ (blue) and deviating simulation results for the given parameter values.

8. Fit Curve Collection

In this section, collections of fit curves for all triads are presented. The parameter sets correspond to the values given in Table 2. For k_S and T_{long}, the combinations shown in Fig. S23 are equivalent. In case of the compounds with low *J*, there are systematic deviations between observed and simulated decay curves in the first ca. 50 ns. They are due to the fact that the quantum calculations show an initial delay of the decay, due to coherence effects in the S/T conversion. To find the optimum fit parameter, the quantum curves were shifted by a few ns to negative time, to suppress the slow initial stage, which is not present in the observed decay curves.

8.1 Me0

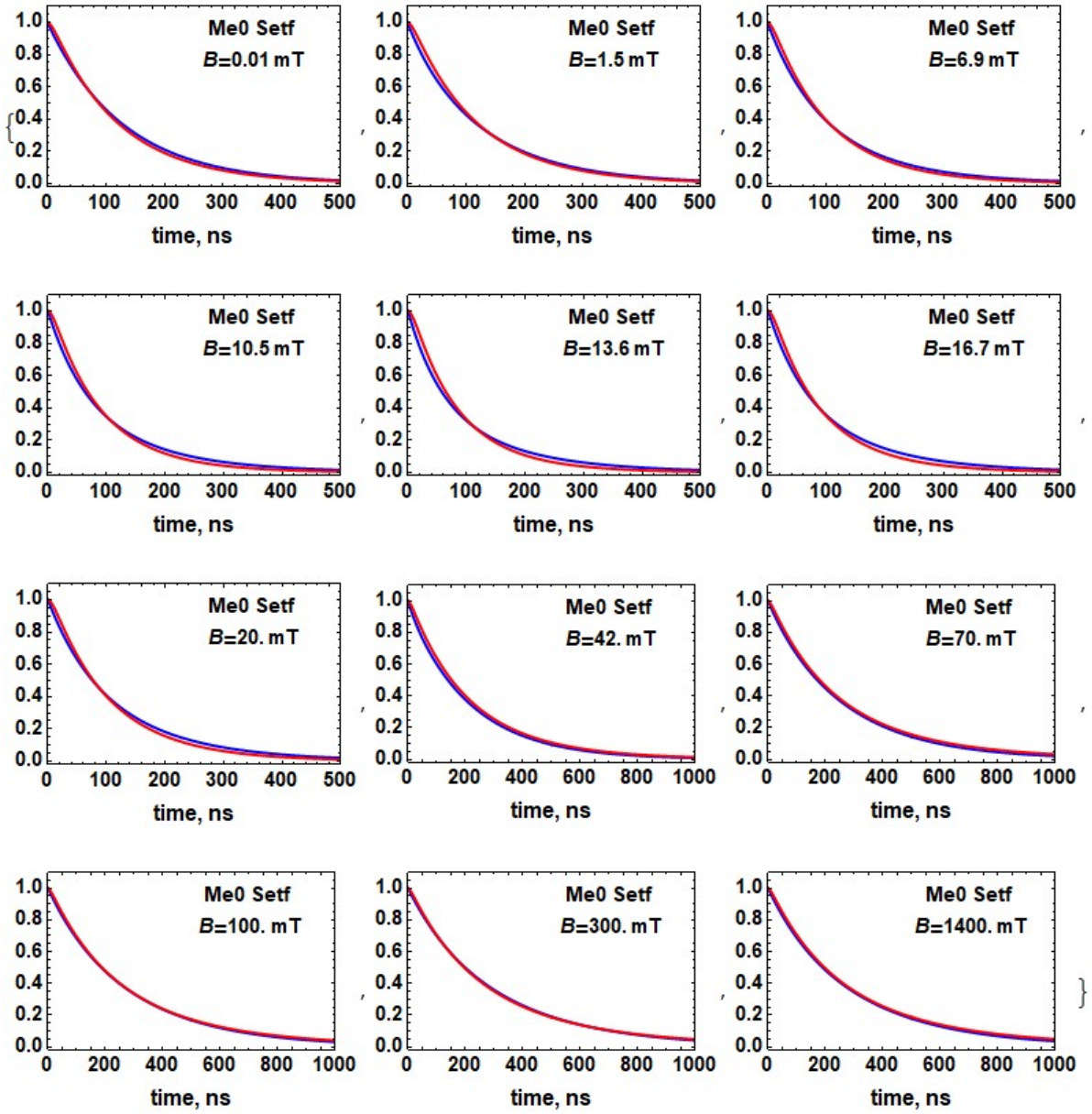

Fig. S26 Experimental (blue) and quantum calculations (red) of the CS decay curves at selected magnetic fields for **Me0**.

8.2 Me2

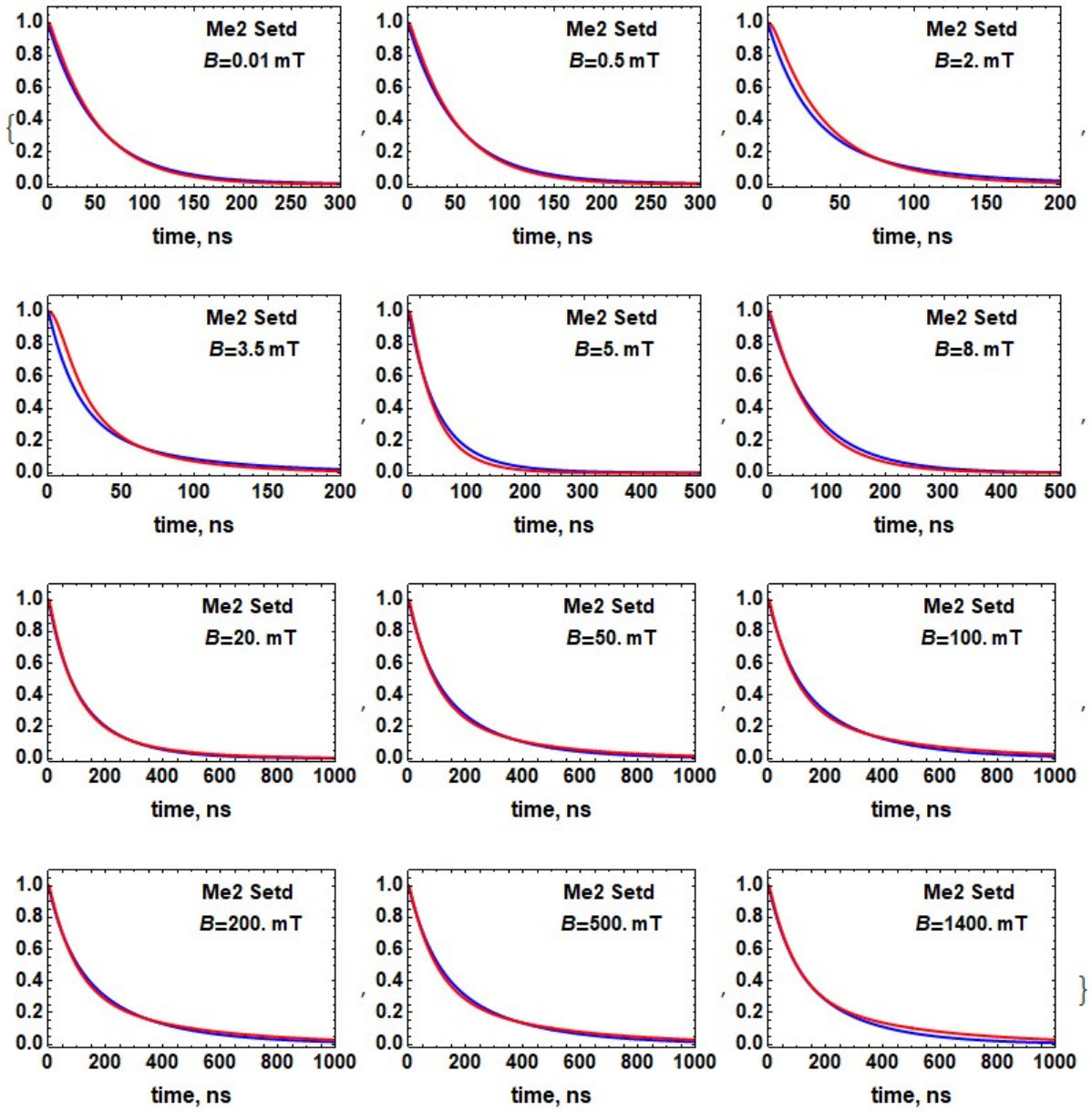

Fig. S27 Experimental (blue) and quantum calculations (red) of the CS decay curves at selected magnetic fields for **Me2**.

8.3 Me3

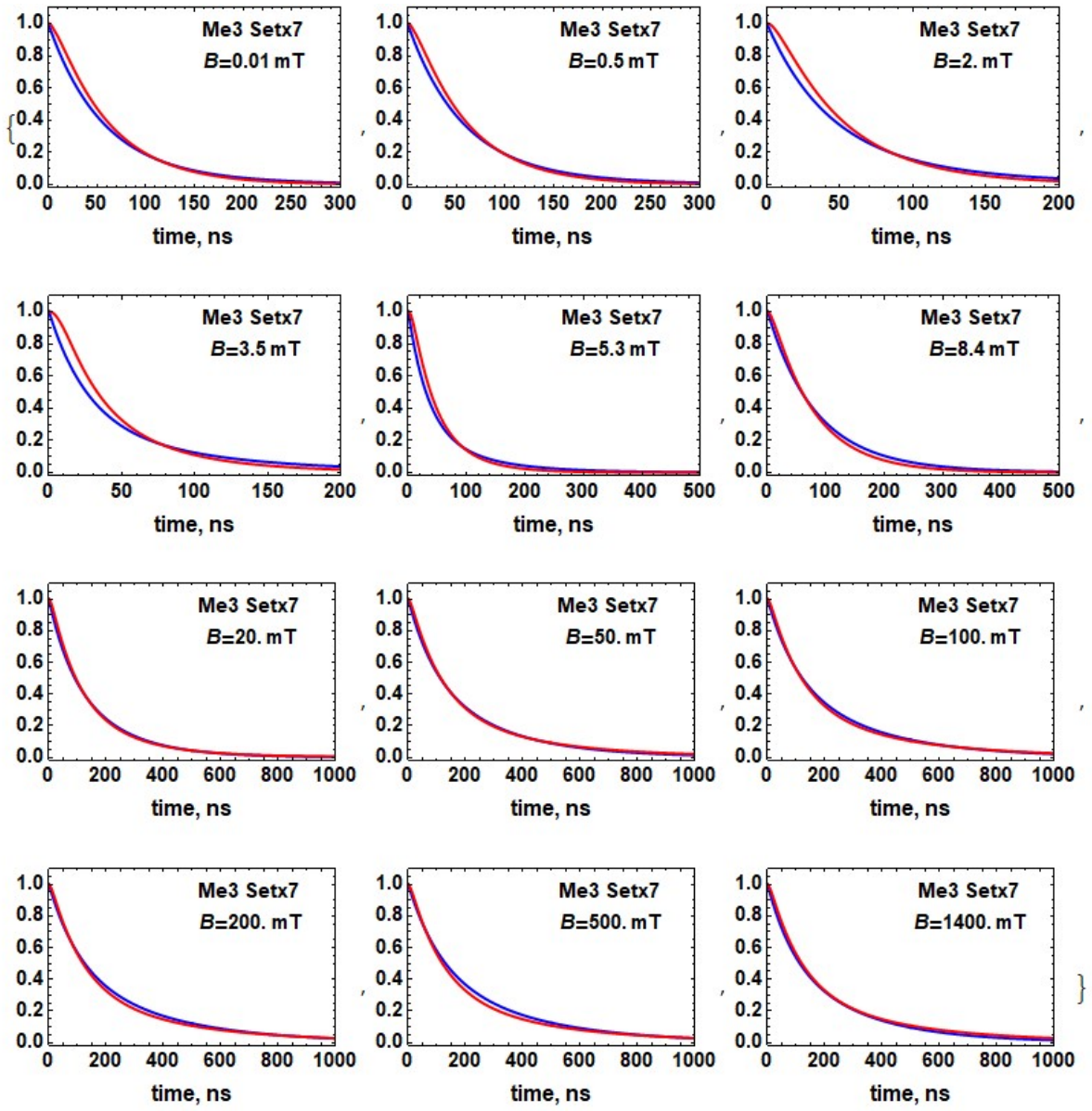

Fig. S28 Experimental (blue) and quantum calculations (red) of the CS decay curves at selected magnetic fields for **Me3**.

8.4 Me23

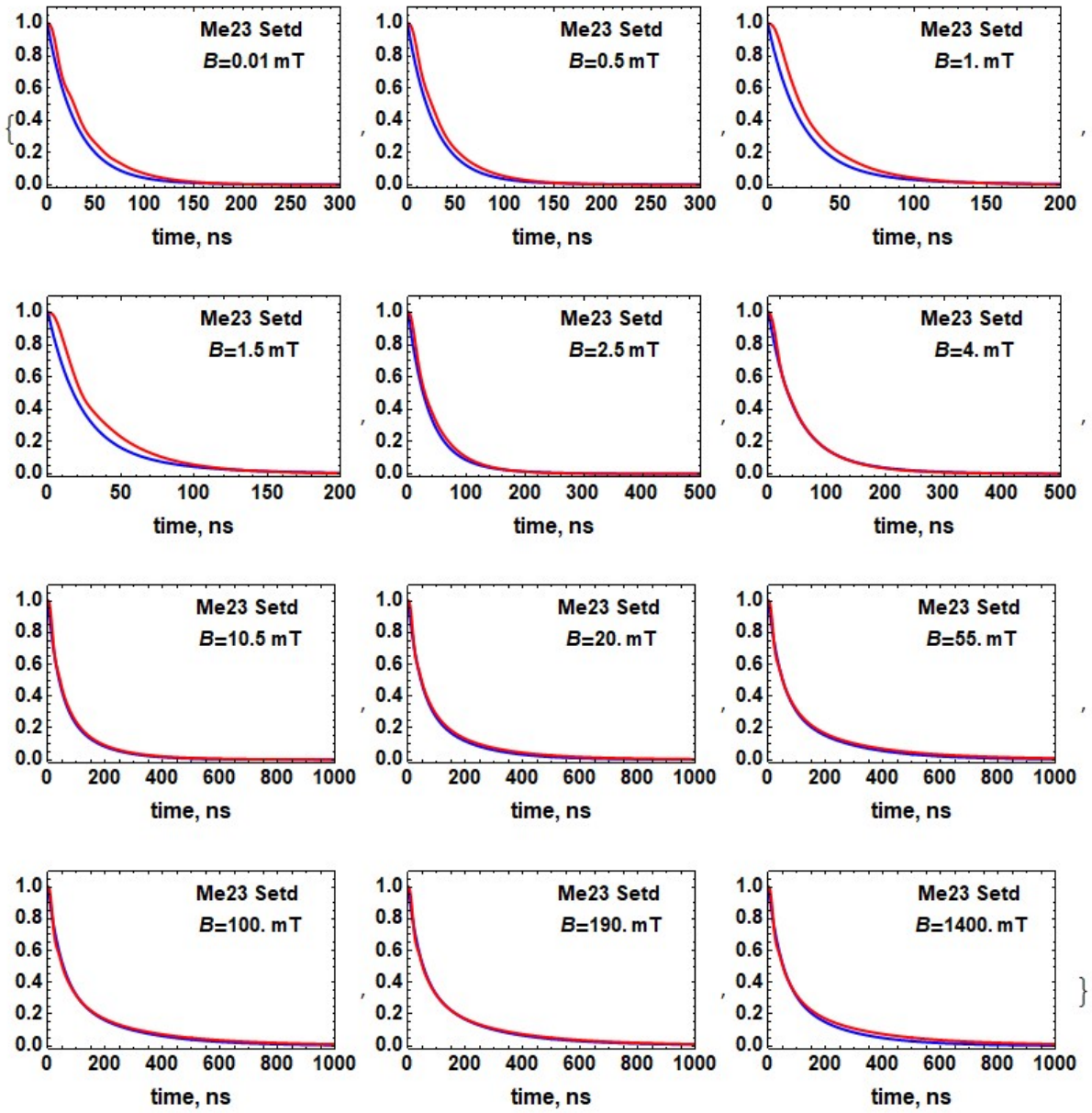

Fig. S29 Experimental (blue) and quantum calculations (red) of the CS decay curves at selected magnetic fields for **Me23**.

9. Orphan States

The matrix in Table 6 represents the coupling between the singlet and the triplet hyperfine states of the radical pair, as caused by the hyperfine coupling with the amine nitrogen in the donor. With a value of a_N = 0.93 mT, the latter largely dominates the total of all hyperfine couplings in the system. From the Table it follows that the $I_{Nz}0$ hyperfine state of the singlet is only coupled with T_+ and T_-. At high fields, these couplings are suppressed due to the Zeeman splitting of the triplet sublevels. Thus, $SI_{Nz}0$ becomes essentially isolated from the triplet and

cannot react, except via the slow relaxation processes.

Table S6 Hyperfine coupling scheme of singlet with triplet hyperfine states of N(TAA).

	$T_+I_{Nz}1$	$T_+I_{Nz}0$	$T_+I_{Nz}-1$	$T_0I_{Nz}1$	$T_0I_{Nz}0$	$T_0I_{Nz}-1$	$T_-I_{Nz}1$	$T_-I_{Nz}0$	$T_-I_{Nz}-1$
$SI_{Nz}1$	0	$-a_N/2$	0	$a_N/2$	0	0	0	0	0
$SI_{Nz}0$	0	0	$-a_N/2$	0	0	0	$a_N/2$	0	0
$SI_{Nz}-1$	0	0	0	0	0	$-a_N/2$	0	$a_N/2$	0

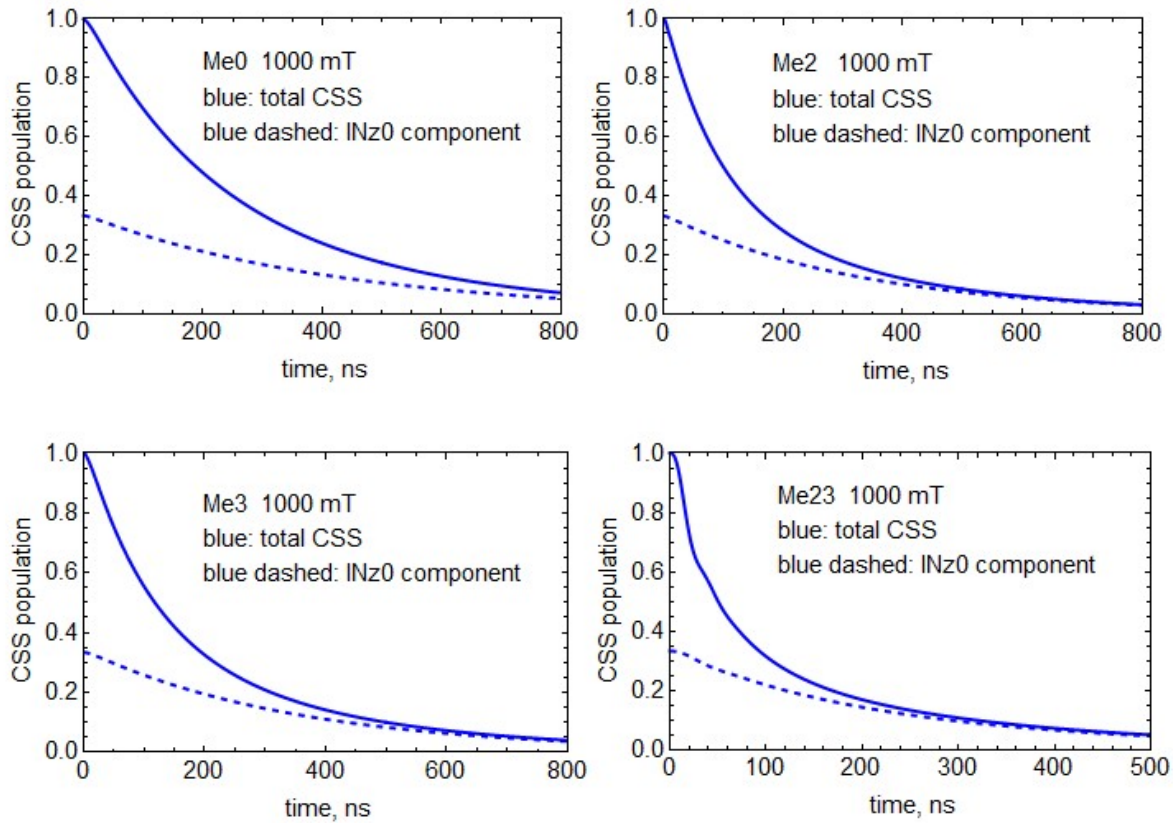

Fig. S30 Decay profiles of CS state at 1000 mT in the series **Me0, Me2, Me3, Me23** simulated by quantum dynamics including 5 nuclei. Blue solid line: total CS population, blue dashed line: population of hyperfine component $SI_{Nz}0$

As is shown in Fig. S30 for a field of 1000 mT, during decay of the CS state the hyperfine component $SI_{Nz}0$ is continuously enriched. For the triads with smaller value of *J*, the enrichment is almost complete after 200 – 400 ns.

10. Potentials and Dynamic Treatment of Intramolecular Twisting

The potentials of intramolecular twisting obtained by DFT calculations are approximated by the analytical functions whereby U1 refers to the rotation between unit 1 and 2 (see Fig. S32), U2 to rotation between 2 (without methyl groups) and 3, U3 to 3 and 4 (without methyl groups), U4 to rotation between 4 and 5, U2Me to rotation between 2 (with methyl groups) and 3, and U3Me to rotation between 3 and 4 (with methyl groups):

```
U1[θ_] = 3.59 + E^(-100. θ^2) + 4 E^(-33.33 (-1.8 + Sqrt[θ^2])^2) -
    2.83 Cos[2 θ] + 3.80 Cos[4 θ] - 0.25 Cos[6 θ] + 0.83 Cos[8 θ];
U2[θ_] = 3.20 - 3.69 Cos[2 θ] + 2.09 Cos[4 θ] + 0.16 Cos[6 θ] +
    0.15 Cos[8 θ] + 0.05 Cos[10 θ];

U3[θ_] = 1.94 + 0.1 E^(-5. θ^2) + 0.031 θ^2 - 0.89 Cos[2 θ] +
    1.81 Cos[4 θ] + 0.32 Cos[6 θ] + 0.17 Cos[8 θ] + 0.075 Cos[10 θ];
U4[θ_] = 3.71 + 5.28 Cos[2 θ] + 3.20 Cos[4 θ] + 0.92 Cos[6 θ] +
    0.43 Cos[8 θ] + 0.25 Cos[10 θ];
U3Me[θ_] = 8.20 + 11.96 Cos[2 θ] + 5.15 Cos[4 θ] + 1.87 Cos[6 θ] + 0.50 Cos[8 θ];
U2Me[θ_] = 4.76 + 7.5 E^(-10. θ^2) + 5.7 E^(-10. (-π + θ)^2) +
    0.50 θ + 7.99 Cos[2 θ] + 3.31 Cos[4 θ] + 0.74 Cos[6 θ] + 0.20 Cos[8 θ];
```

The diagrams are shown in Fig. S31:.

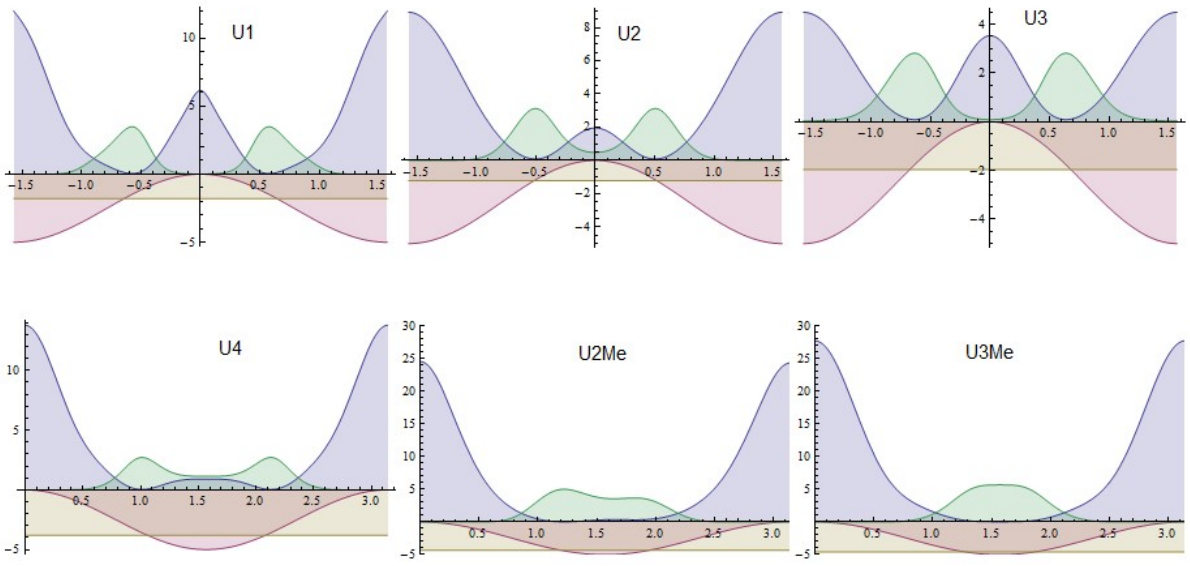

Fig.S31 Blue: potentials in units of k_T versus rotational angle in radians. Green: equilibrium distribution (multiplied by an arbitrary factor of 3), red: $Cos(q)^2$ (shifted by -1 and multiplied by arbitrary factor of 5), horizontal line: average of $Cos(q)^2$,(shifted by -1 and multiplied by an arbitrary factor of 5)

11. Molecular Dynamics of Internal Rotations

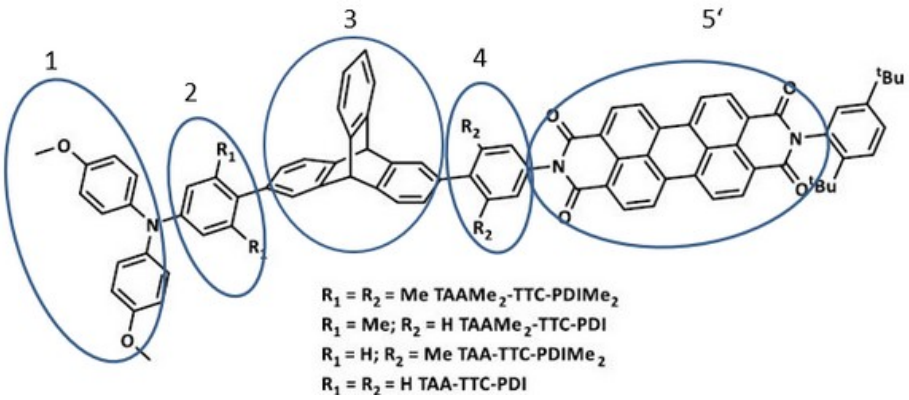

Fig. S32 Definition of the five intramolecular rotors

We consider 5 intramolecular rotors as shown in Fig. S32. With the exception of unit 3, the TTC moiety, each of them can rotate independently around the single bond or pairs of single bonds, respectively, connecting them to its neighbours. For the inner rotors free individual rotation requires a collinearity of the two connecting bonds. For the TTC unit, such a collinearity is not the case (cf. Fig. S33), Therefore it was considered as static with respect to the rotation of the attached phenyl rotor.

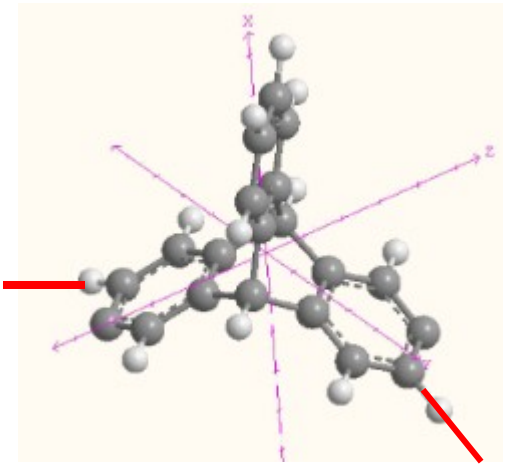

Fig. S33 Connectivity of TTC unit within the triad chain.

For the other rotors, free, uniaxial rotations were considered, described by the following rotational diffusion constants estimated by means of the Einstein Debye relation with effective hydrodynamic radii following from calculations of solvent excluded volumes:

Rotational diffusion constants in toluene : η = 0.57 cP

$D_{rot} = k_B T / 8\pi\eta R^3$

1: 158.1 A^3	R = 335 pm	Drot = 7.87 ns^{-1}
2-Me: 104.7 A^3	R = 292 pm	Drot = 11.9 ns^{-1}
2-H: 71.3 A^3	R = 257 pm	Drot = 17.4 ns^{-1}
3: independent rotation neglected because of non-collinear connectivity		
4-Me: 104.7 A^3	R = 292 pm	Drot = 11.9 ns^{-1}
4-H: 71.3 A^3	R = 257 pm	Drot = 17.4 ns^{-1}
5' 238.2 A^3	R = 384 pm	Drot = 5.02 ns^{-1}

The treatment of the rotational dynamics essentially follows the method given by Grozema et al.[19] However, the individual rotational angles at the various links were not considered as independent since the rotation of any internal moiety changes two of such angles simultaneously.

Torques derived from the potentials:

```
FU1[θ_] = -U1'[θ];
FU2[θ_] = -U2'[θ];
FU3[θ_] = -U3'[θ];
FU4[θ_] = -U4'[θ];
```

Drift terms given as functions of rotation angles φ_i of individuals rotors.
Positive direction defined as mathematically positive when looking from donor to acceptor

```
Δφdrift1[φ1_, φ2_] := -Drot1 * FU1[φ2 - φ1] * Δt;
Δφdrift2[φ1_, φ2_, φ3_] := Drot2 * (FU1[φ2 - φ1] - FU2[φ3 - φ2]) * Δt;
Δφdrift4[φ3_, φ4_, φ5_] := Drot4 * (FU3[φ4 - φ3] - FU4[φ5 - φ4]) * Δt;
Δφdrift5[φ4_, φ5_] := Drot5 * FU4[φ5 - φ4] * Δt;
Δφdrift3[φ2_, φ3_, φ4_] := 0 (*Drot3*(FU2[φ3-φ2]-FU3[φ4-φ3])*Δt*);
```

time unit: 1 ns
time step 0.1 ps: $\Delta t = 0.0001$

Dynamics of coupled rotations:

The diffusional jumps were adjusted for compliance with the condition
$< (\Delta\varphi^2_{diff}> = 2 D_{rot} \Delta t$

```
Do[
   (Dφ[[1]] = Δφdrift1[φ0[[1]], φ0[[2]]] +
      Sqrt[24 * Drot1 * Δt] * 0.288 * RandomVariate[NormalDistribution[]];
    Dφ[[2]] = Δφdrift2[φ0[[1]], φ0[[2]], φ0[[3]]] +
      Sqrt[24 * Drot2 * Δt] * 0.288 * RandomVariate[NormalDistribution[]];
    Dφ[[3]] = 0;
    Dφ[[4]] = Δφdrift4[φ0[[3]], φ0[[4]], φ0[[5]]] +
      Sqrt[24 * Drot4 * Δt] * 0.288 * RandomVariate[NormalDistribution[]];
    Dφ[[5]] = Δφdrift5[φ0[[4]], φ0[[5]]] + Sqrt[24 * Drot5 * Δt] *
       0.288 * RandomVariate[NormalDistribution[]];
```

```
 φ0 += Dφ;
 φTab[[i]] = φ0;
 ΔφTab[[i]] =
   {φ0[[2]] - φ0[[1]], φ0[[3]] - φ0[[2]], φ0[[4]] - φ0[[3]], φ0[[5]] - φ0[[4]]}
), {i, 2, 1 000 000}];
```

12. *J*-Trajectories and Estimation of k_{STD}

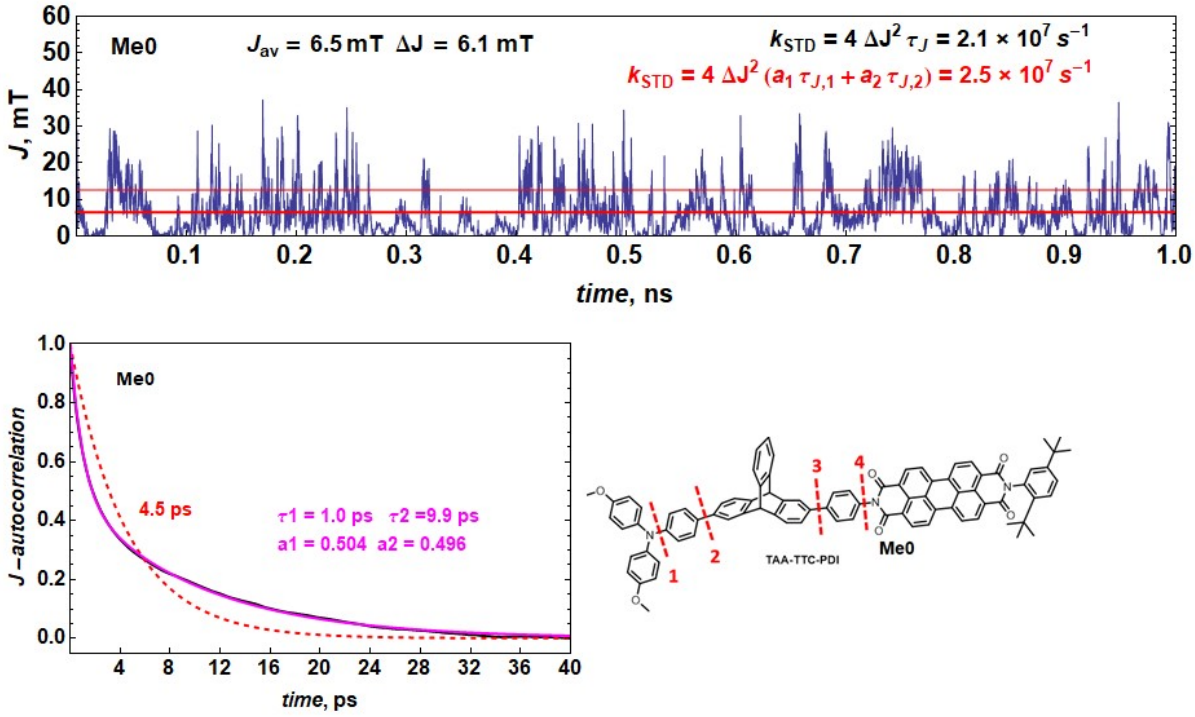

Fig. S34 Trajectory of *J*-values (top) from dynamic simulations and autocorrelation curve with monoexponential and biexponential fit (bottom) for **Me0**.

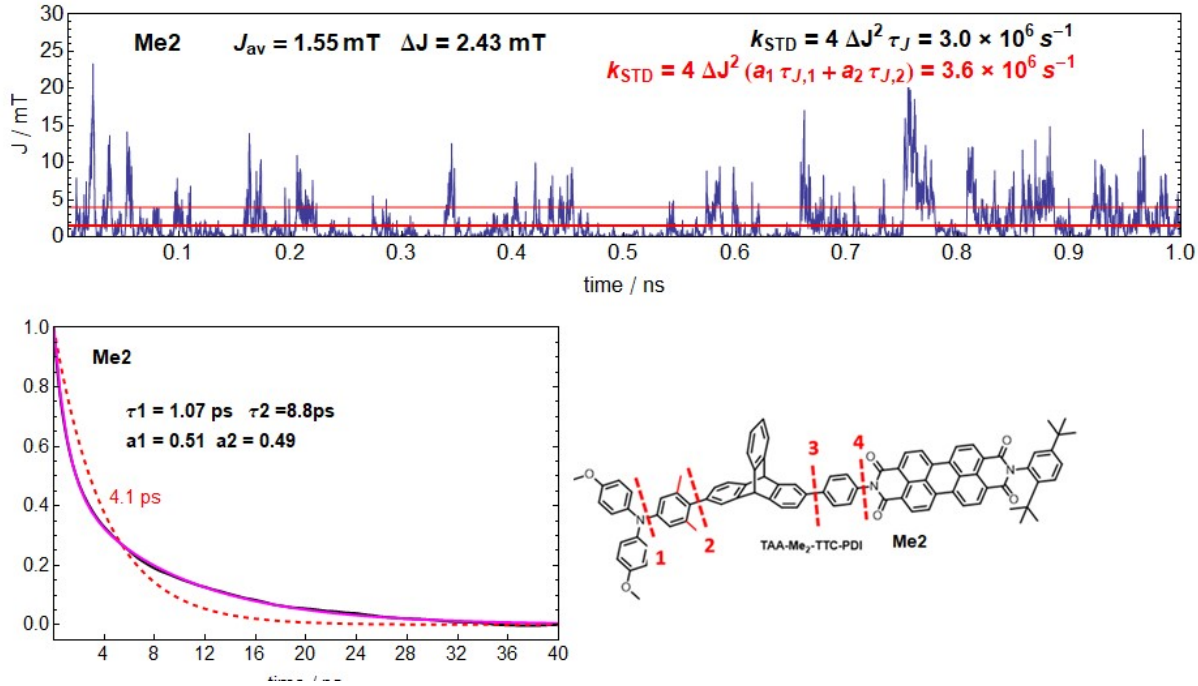

Fig. S35 Trajectory of *J*-values (top) from dynamic simulations and autocorrelation curve with monoexponential and biexponential fit (bottom) for **Me2**.

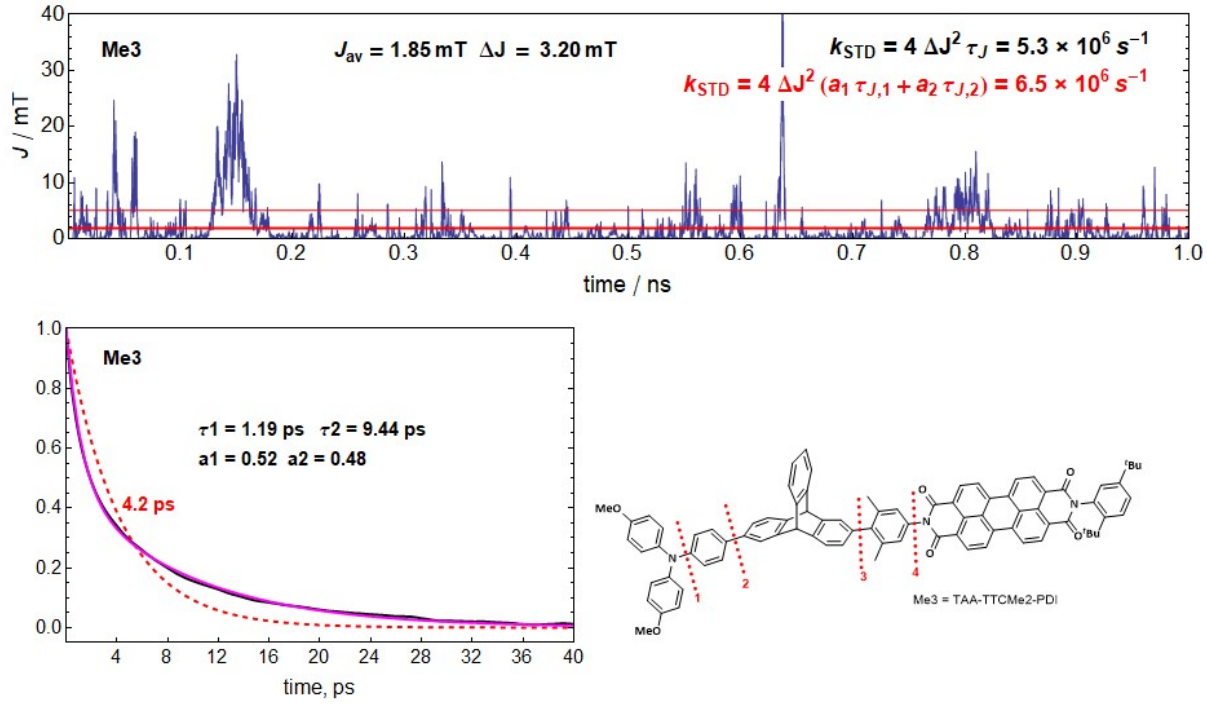

Fig. S36 Trajectory of *J*-values (top) from dynamic simulations and autocorrelation curve with monoexponential and biexponetial fit (bottom) for **Me3**.

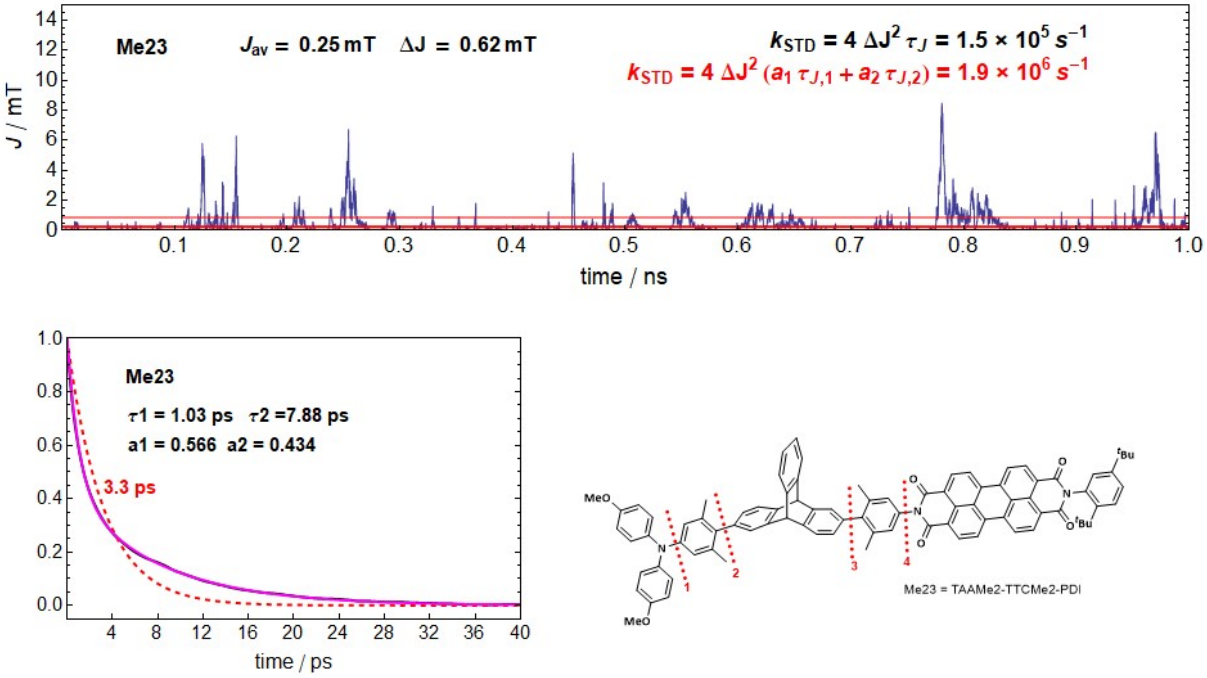

Fig. S37 Trajectory of *J*-values (top) from dynamic simulations and autocorrelation curve with monoexponential and biexponential fit (bottom) for **Me23**.

13. Optimization of Ratio ΔJ / J_{av} by Harmonic Shaping of the Potential

The ratio of ΔJ / J_{av} becomes largest for potentials with their minima close to $\pi/2$ because here the average of cosine-square becomes very small. In Fig. S38 we show the comparison of the results for angle 4, where the connected moieties tend to a perpendicular arrangement.

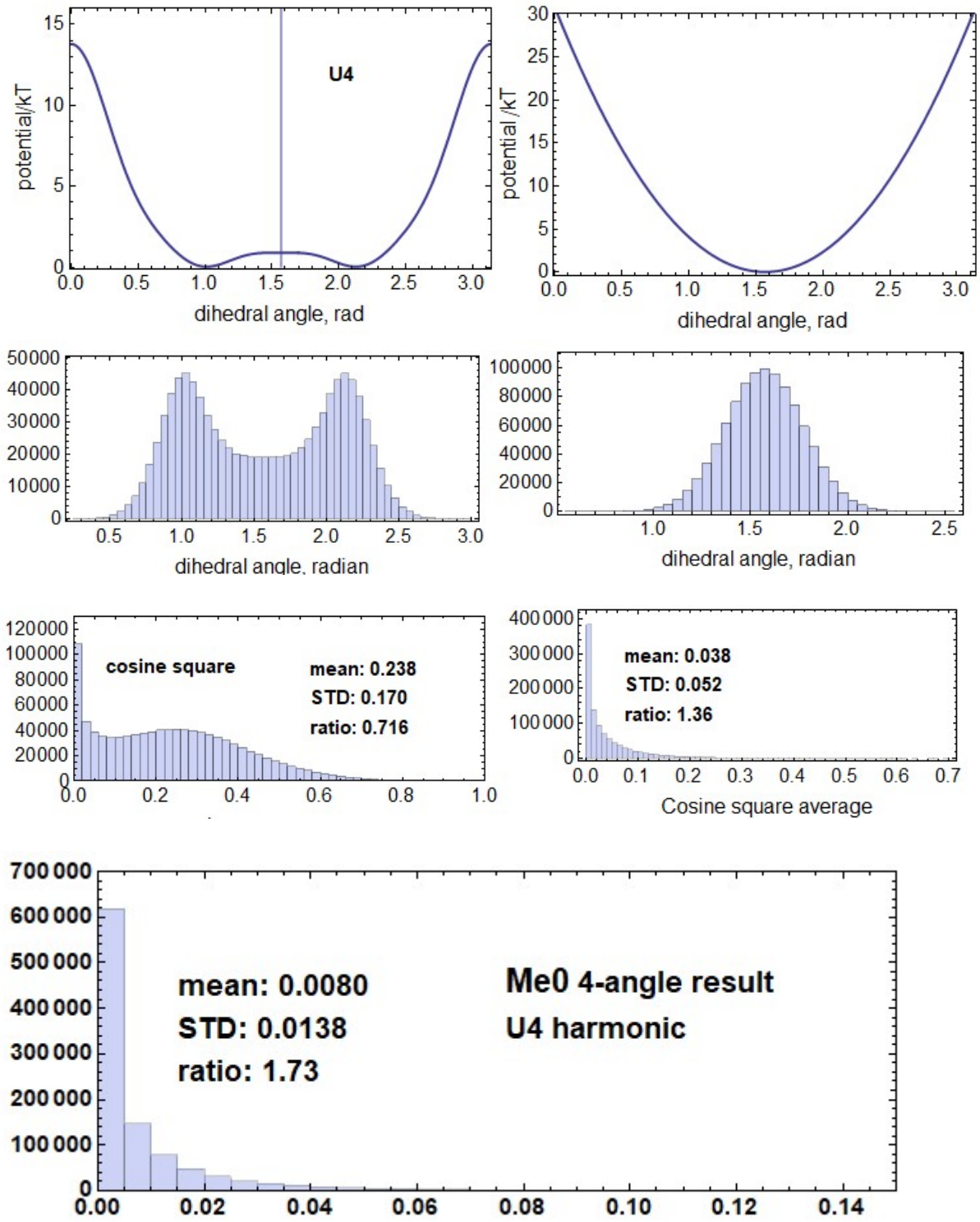

Fig.38 Comparison of angular equilibrium distribution for angle 4 in **Me0** (left column) with a tentative harmonic potential (right column). Lowest line: result for 4-angle combination with the DFT potential of angle 4 replaced by the harmonic potential.

The Fig. 38 shows, how by concentration of the angular distribution around the position of $\pi/2$ the ratio of ΔJ / J_{av} can be largely increased. The achievable ratio, however, seems far from the value of about 8 required to bring ΔJ into the range necessary for a rate constant k_{STD} value in the right order of magnitude.

14. Correlation of Electronic Couplings

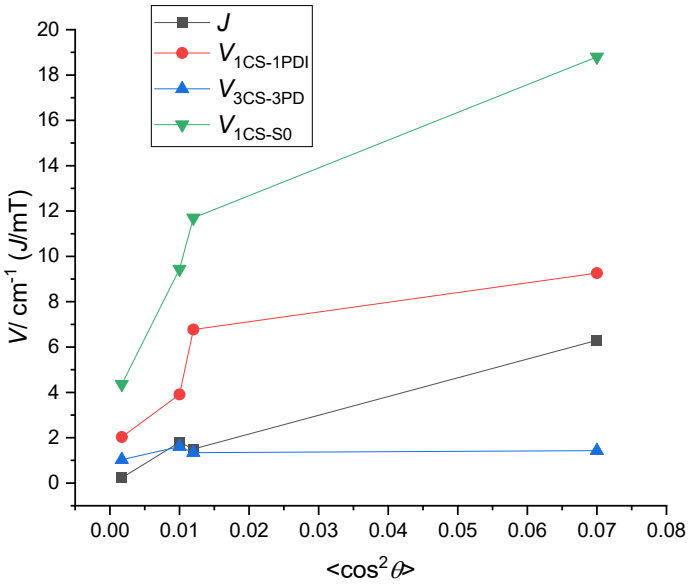

Fig. S39 Correlation of electronic and exchange couplings with average squared cosine of torsion angles.

15. Rate constant of S/T-dephasing by phase integration

The equation of motion for the off-diagonal DM element, characterizing “coherence” in a two-level (e.g. S/T_0) system is given by

$$\rho_{ST_0}(t) = c_S(t)c_{(T_0^*)}(t) = \rho_{ST_0}(0)\exp\left[i\int_0^t J(t')dt'\right] \quad (2)$$

Here $\int_0^t J(t')dt'$ is called “the phase”. For constant *J,* the phase grows linearly in time which corresponds to a pure harmonic oscillation of the matrix element.

Due to the intramolecular rotational motions, *J* is not a constant, but fluctuates in time. Its trajectory can be obtained as a result from a molecular dynamic calculation describing the solvent as a homogeneous viscous medium. For example, a 1 ns section for Me0 looks like shown in Fig. S40.

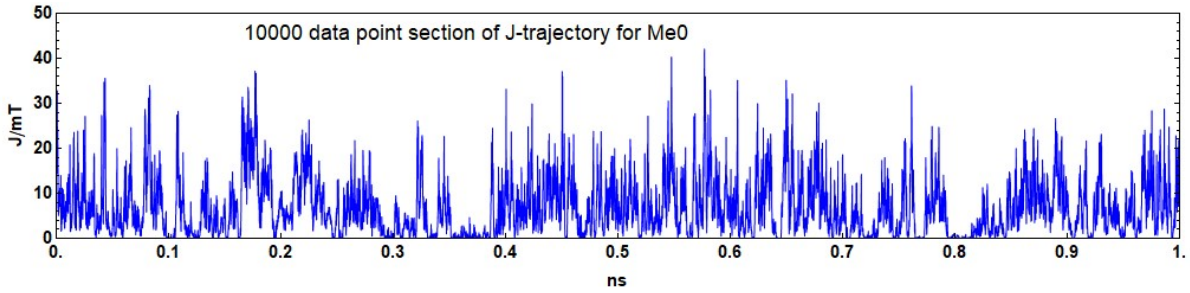

Fig. S40 Sample of J-trajectory for compound Me0

A statistics of the time dependence of the phase integral over 100 trajectories, each one comprising 10000 time steps of 0.1 ps is shown in Figure S41.

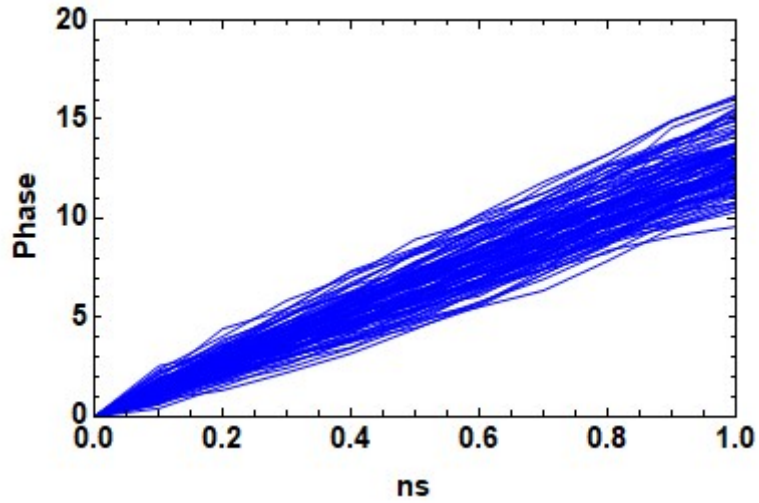

Fig. S41 100 samples of phase evolution (recorded after every 0.1 ns) for Me0.

Eq. (2) is valid for a single trajectory. Taking the average < > over an ensemble of trajectories yields

$$\rho_{ST_0}(t) = \rho_{ST_0}(0)\left\langle \exp\left[i \int_0^t J(t')dt' \right] \right\rangle \tag{3}$$

It is found that the statistics of phase evolution is described by the equation:

$$\phi(t) = \int_0^t J(t')dt' = J_0 t + rnd[N(\sigma_t)] \tag{4}$$

Where the statistical distribution oft the fluctuating part corresponds to a normal distribution with a width of σ_t growing in time according to the Einstein square root law:

$$\sigma_t(t) = \alpha\sqrt{t} \tag{5}$$

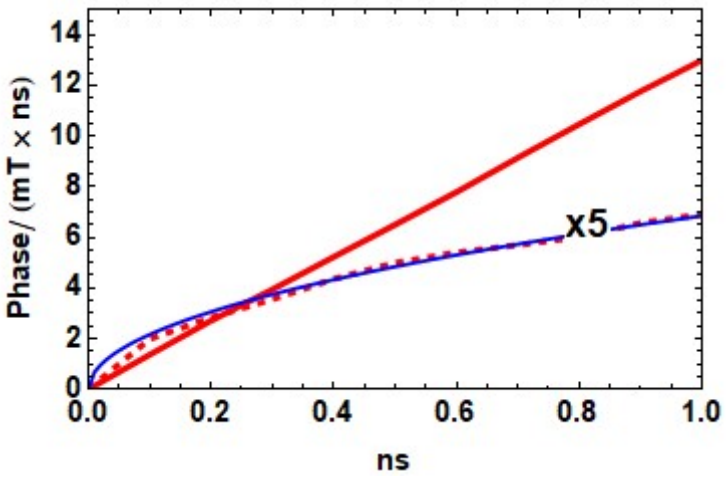

Fig. S42 Evolution of phase. Red: average, red dashed: rms deviation, blue: fit of rms deviation by square root law

Substituting eqs. (4) and (5) into eq. (3) yields

$$\rho_{ST_0}(t) = \rho_{ST_0}(0)\exp\,[iJ_0 t]\int_{-\infty}^{\infty}\frac{e^{-x^2/2\sigma_t^2}}{\sigma_t\sqrt{2\pi}}e^{ix}dx \tag{6a}$$

$$= \rho_{ST_0}(0)\exp\,[iJ_0 t]\exp\,[-\sigma_t^2/2] \tag{6b}$$

$$= \rho_{ST_0}(0)\exp\,[iJ_0 t]\exp\,[-\alpha^2 t/2] \tag{6c}$$

The coherence thus is represented by a constantly oscillating term multiplied by a damping factor $\exp\,[-\alpha^2 t/2]$ with a decay constant of

$$k_{STD} = \alpha^2/2 \tag{7}$$

For Me0 it is found that □ = 1.37 mT ns$^{1/2}$, which corresponds to

$$k_{STD} = \frac{(1.37\ mT \times \sqrt{ns})^2}{2} = (1.37 * 0.176)^2/2\ ns^{-1} = 0.029\ ns^{-1} = 2.9 \times 10^7 s^{-1}$$

a result close to the value of 2.5 × 10^7 s^{-1} obtained by perturbation theory.16

16. References

1. D. Mims, A. Schmiedel, M. Holzapfel, N. N. Lukzen, C. Lambert and U. E. Steiner, *J. Chem. Phys.*, 2019, **151**, 244308.
2. H. Kang, H. Shin, B. Kim and J. Park, *J. Nanosci. Nanotechnol.*, 2016, **16**, 3045-3048.
3. J. C. C. Atherton and S. Jones, *Tetrahedron*, 2003, **59**, 9039-9057.
4. L. Friedman and F. M. Logullo, *J. Am. Chem. Soc.*, 1963, **85**, 1549-1549.
5. Z. Chen and T. M. Swager, *Macromolecules*, 2008, **41**, 6880-6885.
6. N. Miyaura and A. Suzuki, *J. Chem. Soc., Chem. Commun.*, 1979, DOI: 10.1039/C39790000866, 866-867.
7. K. Hu, A. D. Blair, E. J. Piechota, P. A. Schauer, R. N. Sampaio, F. G. L. Parlane, G. J. Meyer and C. P. Berlinguette, *Nature Chemistry*, 2016, **8**, 853-859.
8. C. Würth, M. Grabolle, J. Pauli, M. Spieles and U. Resch-Genger, *Nature Protocols*, 2013, **8**, 1535-1550.
9. A. Weller, *Z. Phys. Chem.*, 1982, **133**, 93-98.
10. PerkinElmer, *Chem3D Ultra, Version 20.0.0.41,*, PerkinElmer Informatics, Inc.
11. M. J. M. J. Frisch, G. W. G. W. Trucks, H. B. Schlegel, G. E. Scuseria, M. A. Robb, J. R. Cheeseman, G. Scalmani, V. Barone, B. Mennucci, G. A. Petersson, H. Nakatsuji, M. Caricato, X. Li, H. P. Hratchian, A. F. Izmaylov, J. Bloino, G. Zheng, J. L. Sonnenberg, M. Hada, M. Ehara, K. Toyota, R. Fukuda, J. Hasegawa, M. Ishida, T. Nakajima, Y. Honda, O. Kitao, H. Nakai, T. Vreven, J. Montgomery, J. E. P. J. A., F. Ogliaro, M. Bearpark, J. J. Heyd, E. Brothers, K. N. Kudin, V. N. Staroverov, R. Kobayashi, J. Normand, K. Raghavachari, A. Rendell, J. C. Burant, S. S. Iyengar, J. Tomasi, M. Cossi, N. Rega, N. J. Millam, M. Klene, J. E. Knox, J. B. Cross, V. Bakken, C. Adamo, J. Jaramillo, R. Gomperts, R. E. Stratmann, O. Yazyev, A. J. Austin, R. Cammi, C. Pomelli, J. W. Ochterski, R. L. Martin, K. Morokuma, V. G. Zakrzewski, G. A. Voth, P. Salvador, J. J. Dannenberg, S. Dapprich, A. D. Daniels, Ö. Farkas, J. B. Foresman, J. V. Ortiz, J. Cioslowski and D. J. Fox, *Gaussian 09, Version B.01*, Gaussian, Inc., Wallingford CT, 2009.
12. S. F. Nelson, S. C. Blackstock and Y. Kim, *J. Am. Chem. Soc.*, 1987, **109**, 677-682.
13. S. F. Nelson, H. Chang, J. J. Wolff and J. J. Adamus, *J. Am. Chem. Soc.*, 1993, **115**, 12276.
14. J. H. Klein, T. L. Sunderland, C. Kaufmann, M. Holzapfel, A. Schmiedel and C. Lambert, *Physical Chemistry Chemical Physics*, 2013, **15**, 16024-16030.

15. C. Kaiser, A. Schmiedel, M. Holzapfel and C. Lambert, *J. Pys. Chem. C.*, 2012, **116**, 15265-15280.
16. J. K. Hurley, N. Sinai and H. Linschitz, *Photochem. Photobiol.*, 1983, **38**, 9-14.
17. I. Zhukov, N. Fishman, A. Kiryutin, N. Lukzen, M. Panov, U. Steiner, H. M. Vieth, J. Schäfer, C. Lambert and A. Yurkovskaya, *J. Chem. Phys.*, 2020, **152**, 014203.
18. D. Mims, J. Herpich, N. N. Lukzen, U. E. Steiner and C. Lambert, *Science*, 2021, **374**, 1470-1474.
19. Y. A. Berlin, F. C. Grozema, L. D. A. Siebbeles and M. A. Ratner, *Journal of Physical Chemistry C*, 2008, **112**, 10988-11000.